

Correlation engineering via non-local dissipation

K. Seetharam*^{1,2} A. Lerose,³ E. J. Davis,^{4,5} R. Fazio,^{6,7} and J. Marino^{2,8}

¹*Department of Electrical Engineering, Massachusetts Institute of Technology, Cambridge, Massachusetts 02139, USA*

²*Department of Physics, Harvard University, Cambridge MA, 02138, USA*

³*Department of Theoretical Physics, University of Geneva, 1211 Geneva, Switzerland*

⁴*Department of Physics, University of California, Berkeley, California 94720 USA*

⁵*Department of Physics, Stanford University, Stanford, CA 94305, USA*

⁶*International Center for Theoretical Physics ICTP, Strada Costiera 11, I-34151, Trieste, Italy*

⁷*Dipartimento di Fisica, Università di Napoli 'Federico II', Monte S. Angelo, I-80126 Napoli, Italy*

⁸*Institut für Physik, Johannes Gutenberg Universität Mainz, D-55099 Mainz, Germany*

Controlling the spread of correlations in quantum many-body systems is a key challenge at the heart of quantum science and technology. Correlations are usually destroyed by dissipation arising from coupling between a system and its environment. Here, we show that dissipation can instead be used to engineer a wide variety of spatio-temporal correlation profiles in an easily tunable manner. We describe how dissipation with any translationally-invariant spatial profile can be realized in cold atoms trapped in an optical cavity. A uniform external field and the choice of spatial profile can be used to design when and how dissipation creates or destroys correlations. We demonstrate this control by preferentially generating entanglement at a desired wavevector. We thus establish non-local dissipation as a new route towards engineering the far-from-equilibrium dynamics of quantum information, with potential applications in quantum metrology, state preparation, and transport.

Correlations in many-body systems allow us to monitor the dynamics of quantum information by giving insight, for example, into the growth of quantum fluctuations and entanglement [1–3]. While dissipation usually decoheres the system, it can also be used to prepare correlated quantum states that are a powerful resource for quantum information processing [4–8]. Compared to the conventional use of unitary processes to manipulate a system, the irreversibility of dissipative dynamics makes it more robust to variations in the initial state and allows for simpler control protocols.

Realizing the potential of dissipation engineering has been challenging, with experiments thus far using a combination of unitary operations and dissipation to produce and stabilize entangled states of a small number of qubits [9–11]. Purely dissipative preparation of correlated states typically requires losses that are non-local in space and can lock the phases of two or more adjacent particles [4]. Experimental implementations of such non-local dissipation have been proposed in atomic platforms, but with limited tunability of the spatial profile [12, 13].

Our work demonstrates a practical route towards dissipative quantum information processing, showing that dissipation with a customizable spatial profile is readily realizable in systems of cold atoms trapped in a single-mode cavity, and furthermore that the behavior of this dissipative channel can be modulated via a uniform external field. Control over the spatial profile and uniform field can be exploited to engineer the profile of correlations in the system, which we show by tailoring the spatio-temporal window over which correlations are present, creating oscillating packets of correlations, and sending the system towards an increasingly squeezed state. The ability to shape correlations enables the manipulation of entanglement dynamics, which we demonstrate by generating entanglement at a target wavevector.

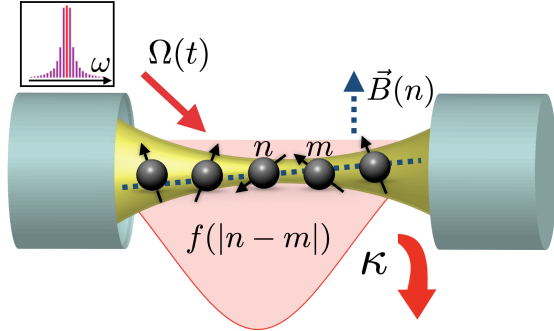


Figure 1. **Experimental realization.** Spin degrees of freedom are encoded in the internal states of atoms trapped in a leaky optical cavity. A magnetic field gradient, $\vec{B}(n)$, and a classical Raman beam, $\Omega(t)$, with multiple sidebands (inset) are used to generate a desired spatial profile, $f(|n - m|)$, of non-local dissipation.

We first illustrate the novel dynamics enabled by non-local dissipation. Consider a translationally-invariant, one-dimensional many-body quantum system undergoing both unitary dynamics and Markovian dissipation. The state of the system, ρ , evolves according to the quantum master equation in Lindblad form

$$\dot{\rho} = i \left[\rho, \hat{H} \right] + \kappa \sum_{n,m} f_{n,m} \left(\hat{L}_n \rho \hat{L}_m^\dagger - \frac{1}{2} \left\{ \hat{L}_m^\dagger \hat{L}_n, \rho \right\} \right), \quad (1)$$

where \hat{H} is the Hamiltonian characterizing unitary evolution, \hat{L}_n is the jump operator characterizing the loss channel, and $n, m = 1 \dots N$ index the sites of the chain. Here, $f_{n,m}$ is the spatial profile of the dissipation and only depends on the difference $|n - m|$. Independent dissipation, corresponding to $f_{n,m} = \delta_{n,m}$, and collective dissipation, corresponding to $f_{n,m} = 1$, are the two commonly considered scenarios. The former is a common

source of decoherence in experiments, while the latter can generate collective entanglement useful for quantum metrology [14–18]. Both these loss channels are spatially homogeneous and therefore cannot cause correlations to spread in space.

The case of tunably non-local dissipation can be understood as interpolating between independent and collective loss. For example, consider a short-range spatial profile, $f_{n,m} = e^{-|n-m|/\chi}$, where χ is the length scale of the profile. If the system is comprised of atoms coupled to a common cavity mode, with dissipation arising from photons leaking out of the cavity, detection of a leaked photon does not allow one to discern which specific atom emitted the photon. Instead, such a photon can only be traced back to a neighborhood of atoms comprised of approximately χ sites. As χ is decreased or increased, we recover independent and collective dissipation respectively.

Figure 1 schematically depicts how to realize non-local dissipation of spin-1/2 systems using cold atoms trapped in a single-mode optical cavity. The spin states are encoded in the hyperfine levels of the atoms and the cavity photon mode allows the atoms to communicate with each other, through both coherent interactions and non-local dissipation. There are three key components to this construction. First, a magnetic field gradient makes the energy of the hyperfine levels site-dependent and thereby endows the system with spatial resolution [19]. Second, a classical Raman beam with multiple sidebands provides control over atomic transitions between different spin states [19, 20]. The frequencies of the sidebands can be chosen so that communication between atoms via the cavity mode only depends on the distance between atoms, thereby enforcing translational invariance. The amplitudes of the sidebands determine the rate of internal atomic transitions and dictate the likelihood that two atoms a fixed distance apart communicate with each other, thereby setting the spatial profile of the dynamical channel. Third, cavity photon losses are large enough that the coherent spin-exchange contribution to dynamics is negligible and only dissipative dynamics remains. The three ingredients described above can be used to construct non-local dissipation channels with a variety of jump operators \hat{L}_n . Experiments will generally suffer from additional local dissipation arising from spontaneous scattering of individual atoms into free space; we derive conditions for the robustness of our set-up to such losses in the Supplementary Information.

In this work, we consider the case of a $\hat{L}_n = \hat{S}_n^-$ dissipation channel with \hat{S}_n^- being the spin lowering operator on site n . Details of the experimental implementation for this channel and the construction a desired spatial profile $f_{n,m}$ are given in the Supplementary Information. Here, we examine the purely dissipative dynamics arising from Eq. 1 with $\hat{H} = 0$. We start the system in a coherent spin state in the northern hemisphere of the collective spin Bloch sphere, parameterized by the initial polar and azimuthal angles $\theta(t=0) = 0.4\pi$ and $\phi(t=0) = 0$, and

compute the dynamics of the equal-time connected correlation function

$$C^{zz}(r, t) = \langle \hat{S}_n^z(t) \hat{S}_{n+r}^z(t) \rangle - \langle \hat{S}_n^z(t) \rangle \langle \hat{S}_{n+r}^z(t) \rangle, \quad (2)$$

which is directly sensitive to the action of spin losses generated by $\hat{L}_n = \hat{S}_n^-$. We also track the evolution of the collective spin, $\langle \hat{S} \rangle = \langle \sum_n \hat{S}_n \rangle$, and the Kitagawa squeezing parameter, $\xi_{k=0}^2 = \frac{4}{N} \min_{e_\perp} \langle \Delta(e_\perp \cdot \hat{S})^2 \rangle$ [21]. In the latter, the minimization of the variance is over directions e_\perp that are perpendicular to the direction of the collective spin. We show the dynamics of these quantities for both long-range and short-range spatial profiles in Fig. 2. Their qualitative behavior is universal. Correlations spread for a period of time before contracting back towards an uncorrelated state as the collective spin crosses the equator of the Bloch sphere and eventually reaches the south pole. The squeezing parameter, which acts as an entanglement witness, drops below one over the course of this motion and signifies the presence of entanglement in the system. The main difference between long- and short-range profiles is that the short-range profile generates correlations that decay more quickly in space at any given time. These dynamics, and the time-dependent spin-wave theory used to compute them, are further characterized in the Supplementary Information. Note that the dynamics is computed for a thermodynamically large number of sites and is plotted over the limited range $r = -10, \dots, 10$ for clarity.

The spread and contraction of correlations is reminiscent of dynamical signatures of confinement in purely unitary spin systems [22–24]. There, correlations are confined due to bound states in the spectrum of Hamiltonian which arise from an effective attractive potential for low-lying excitations. Here, however, confinement of correlations is an inherently non-equilibrium phenomenon stemming from the fact that non-local dissipation channels can both create and destroy correlations.

Intuition for this property can be gained by examining the dynamics of the $\hat{L}_n = \hat{S}_n^-$ channel with long-range profile $f_{n,m} = (|n - m| + 1)^{-\alpha}$, depicted in Fig. 2(a)-(c). In the thermodynamic limit, the system behaves qualitatively as if $\alpha = 0$ for any $\alpha \leq 1$ and exhibits collective dynamics which is fully captured by the motion of the collective spin on a Bloch sphere [25]. For α just above 1, the system is well-described by a collective spin moving along with spin-wave excitations generated on top of it by the spatially dependent spin-lowering jump operator. When the collective spin is in the northern hemisphere of the Bloch sphere, the average magnetization of the system is positive and the jump operator \hat{S}_n^- creates spin-waves by lowering the magnetization away from that of a spin-coherent state which is fully polarized upwards. When the collective spin is in the southern hemisphere of the Bloch sphere, the average magnetization of the system is negative and the jump operator destroys spin-waves by lowering the average magnetization towards that of a spin-coherent state which is fully polarized downwards.

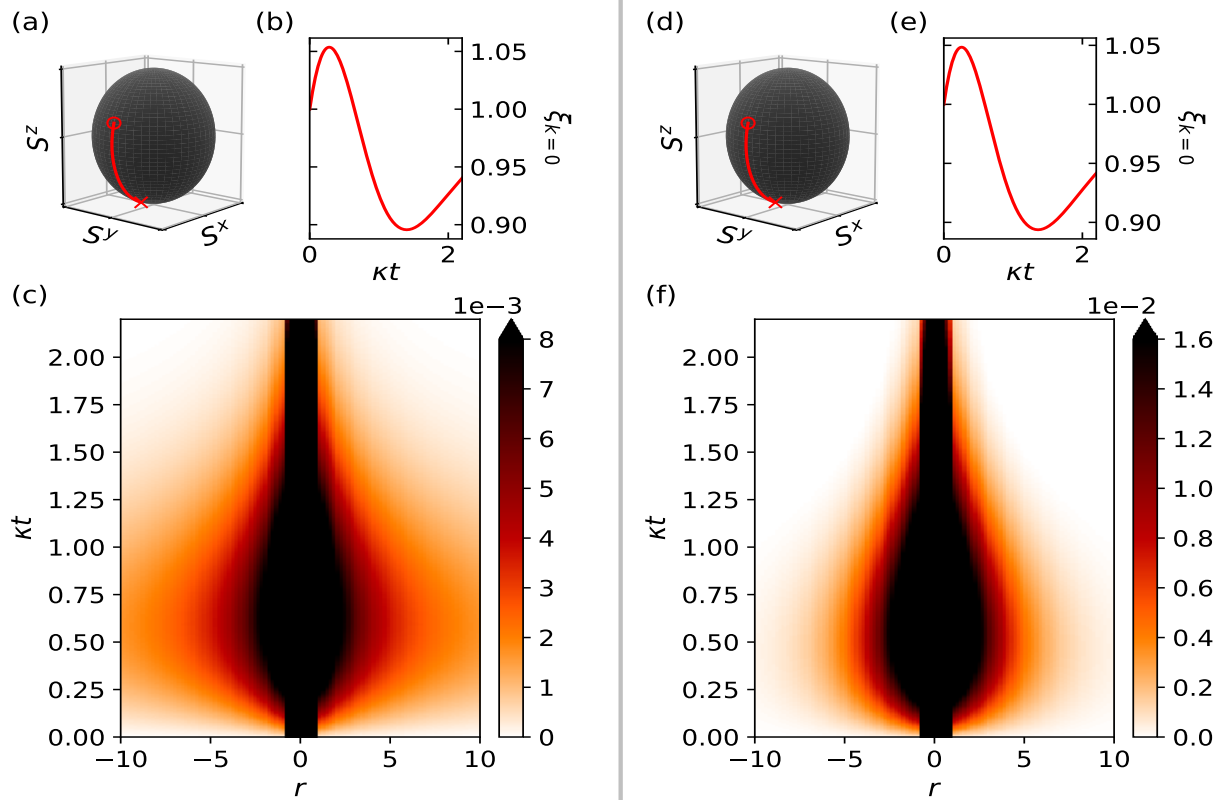


Figure 2. Dynamical confinement via dissipation. Panels (a)-(c) correspond to a long-range spatial profile with $\alpha = 1.25$. Panels (d)-(f) correspond to a short-range spatial profile with $\chi = 2.0$. For both cases, we choose $\kappa = 1$ and initialize the system in a spin coherent state pointing in the direction $\theta(t = 0) = 0.4\pi$, $\phi(t = 0) = 0$. (a), (d) Motion of the collective spin on the Bloch sphere. (b), (e) Squeezing of the collective spin. (c), (f) Connected correlation function $C^{zz}(r, t)$. Correlations spread and then contract in accordance to the motion of the collective spin. Upper bounds are imposed on the color scales to visually highlight correlation profiles.

The collective spin therefore acts as a mobile vacuum for excitations and its position controls whether the dissipation channel predominantly creates or destroys correlations carried by these excitations.

A uniform external field which guides the motion of the collective spin, and thereby influences when dissipation creates or destroys excitations, can be used to modulate the spatio-temporal correlation pattern created by the $\hat{L}_n = \hat{S}_n^-$ dissipation channel. We demonstrate this control using a field of magnitude ω_F and direction φ described by the Hamiltonian $\hat{H} = \omega_F (\cos \varphi \hat{S}^x + \sin \varphi \hat{S}^z)$, which generates the coherent part of dynamics in Eq. 1.

In Fig. 3(a)-(d), we show how the long-range confinement pattern of Fig 2(a)-(c) can be modified. Figure 3(b) shows temporal control over the correlation pattern. The window of time during which the system remains correlated before decaying to an uncorrelated state is extended by a factor of approximately five. This adjustable confinement of correlations demonstrates control over the spatio-temporal window in which information spreads. The pattern in Fig. 3(b) is reminiscent of unitary spin echo protocols as it evolves from an uncorrelated state

to an entangled state, and then back to an uncorrelated state, with an adjustable window of time over which the system is correlated and potentially sensitive to a perturbing field.

Figure 3(d) shows that the confinement pattern can be modulated to exhibit oscillating correlations, which resembles a dissipation-induced limit cycle dressed by quantum fluctuations. This behaviour, however, is metastable and the system reaches a non-oscillatory steady state. For parameters $\alpha \leq 1$, $\varphi = 0$, and $\omega_F \geq \kappa$, the system is fully described by the classical motion of the collective spin and exhibits persistent oscillations [26]. However, for $\alpha > 1$, we find that these oscillations are eventually washed out by many-body fluctuations.

In Fig. 3(e)-(f), we manipulate the short-range confinement pattern of Fig 2(d)-(f) via the uniform field. Specifically, we send the system to an increasingly correlated state at late times. The Kitagawa squeezing parameter, $\xi_{k=0}$, in Fig. 3(e) drops quickly in this case, indicating a progressive improvement in metrological gain.

We also plot the finite wavevector squeezing parameter

$$\xi_k^2 = \frac{4}{N} \min_{e_\perp} \langle \Delta \left(e_\perp \cdot \hat{S}_k \right)^2 \rangle, \quad (3)$$

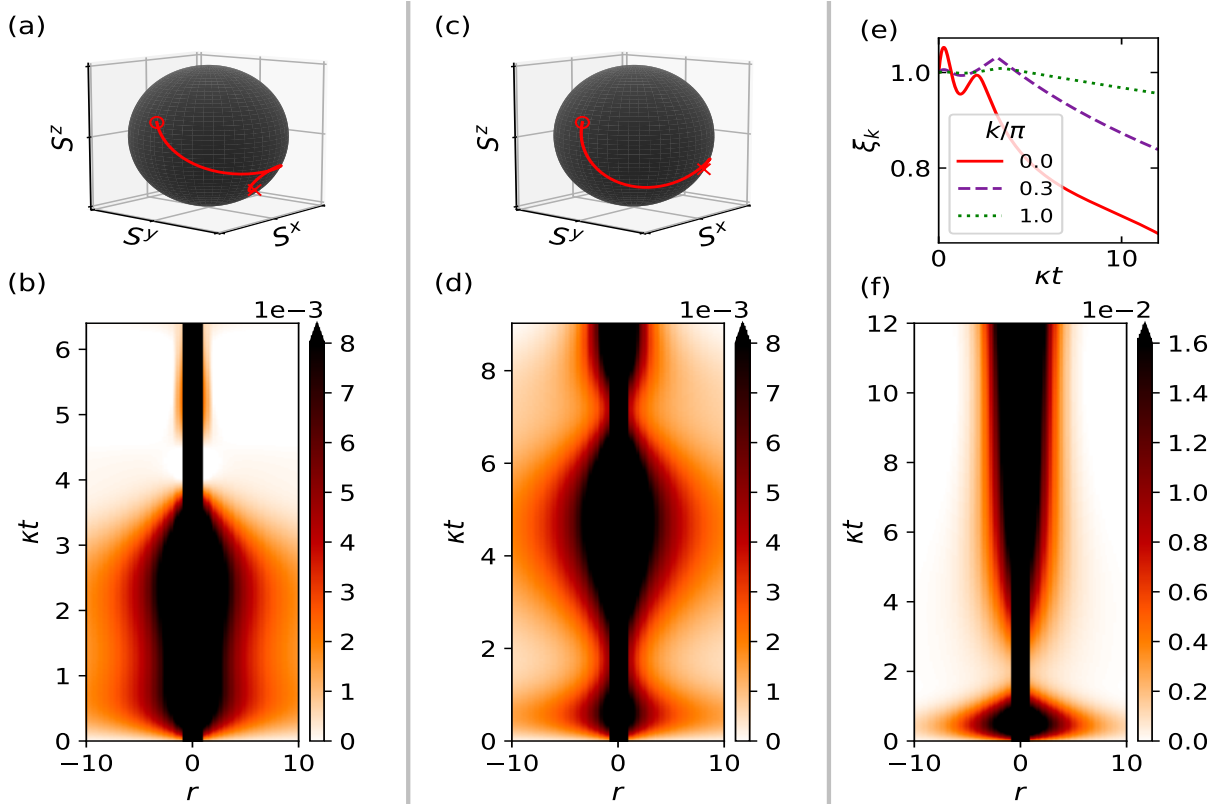


Figure 3. Modulating correlations via a uniform field. We initialize the system in a spin coherent state pointing in the direction $\theta(t=0) = 0.4\pi$, $\phi(t=0) = 0$ for all panels. (a),(b) Collective spin motion and connected correlation function $C^{zz}(r, t)$ for a long-range spatial profile with $\alpha = 1.25$. System parameters are $\kappa = 0.8$, $\omega_F = 1.0$, and $\varphi = 0.25\pi$. (c),(d) Collective spin motion and connected correlation function $C^{zz}(r, t)$ for a long-range spatial profile with $\alpha = 1.1$. System parameters are $\kappa = 0.95$, $\omega_F = 1.0$, and $\varphi = 0.1\pi$. (e),(f) Squeezing parameter and connected correlation function $C^{zz}(r, t)$ for a short-range spatial profile with $\chi = 3.0$. System parameters are $\kappa = 1.2$, $\omega_F = 1.0$, and $\varphi = 0$. Upper bounds are imposed on the color scales to visually highlight correlation profiles.

which is a generalization of $\xi_{k=0}$. This parameter witnesses entanglement at a wavevector k , with applications to spatially resolved measurements of many-particle entanglement in cold atoms [27]. In the Supplemental Information, we show that ξ_k can be related to the uncertainty in the mutual orientation of spins separated by a distance of r sites, which connects the quantity to spatial correlation functions that are commonly measured with fluorescence imaging. Figure 3(e) shows that different wavevectors exhibit varying amounts of squeezing. The relative squeezing of different spatial modes depends on the Fourier transform of the spatial profile, given by $\Gamma_k = \sum_{r=n-m} e^{ikr} f(|r|)$. Modes with larger Γ_k will get squeezed more at short times, as discussed in the Supplementary Information. This fact can be exploited to preferentially squeeze a target mode k^* , thereby generating entanglement at a given wavevector.

We demonstrate this control in Fig. 4, where we show the dynamics of ξ_k for a spatial profile $f_{n,m} = \cos(k^*|n-m|) e^{-|n-m|/\chi}$ with $k^* = 0.3\pi$. The figure inset shows that Γ_k is a Lorentzian of width χ peaked at k^* . We see that the $k = k^*$ mode is squeezed more

than other modes, including the collective $k = 0$ mode which witnesses pairwise entanglement. The correlation dynamics can thus be engineered to generate states which act as a resource of multimode entanglement for quantum information processing tasks.

We have established non-local dissipation as an experimentally realizable and tunable route towards engineering the dynamics of quantum information. Compared to purely unitary strategies, dissipative protocols may hold unique advantages in a variety of applications as irreversible dynamics is stable to variations in the initial state and can naturally drive a system into a correlated regime with simple control schemes.

The tunability of correlation patterns demonstrated in this work may be extended. In Ref. [28], an oscillating magnetic field was used to modulate the spatial symmetries of correlations in a Bose-Einstein condensate. Allowing the uniform external field or Raman sideband amplitudes in our platform to vary over time may similarly provide additional control over correlation dynamics.

The correlation function in Eq. (2) can be experimentally measured by probing higher order spin momenta

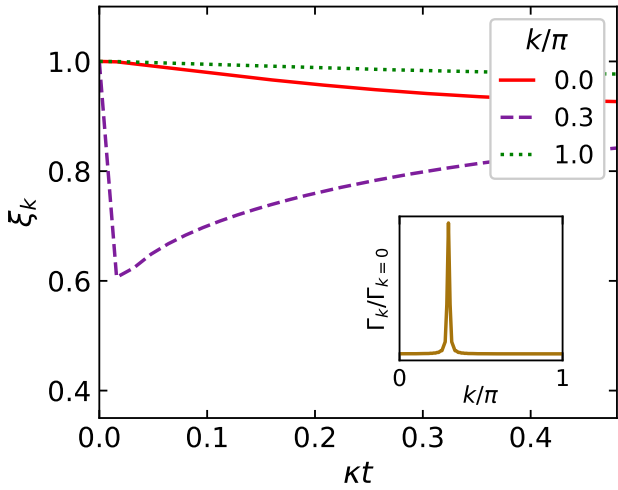


Figure 4. Preferentially squeezing a target wavevector. Spatial squeezing parameter for a spatial profile $f_{n,m} = \cos(k^*|n-m|) e^{-|n-m|/\chi}$ with $\chi = 50$ and $k^* = 0.3\pi$. System parameters are $\kappa = 0.8$, $\omega_F = 1.0$, and $\varphi = 0$. The system is initialized in a spin coherent state pointing in the direction $\theta(t=0) = 0.4\pi$, $\phi(t=0) = 0$. The figure inset shows that the Fourier transform of the spatial profile is peaked around k^* .

via light emitted by the cavity [29]. Initially preparing a non-local spin state alternatively allows one to track the dynamics of the system with direct measurements of the local magnetization [30], potentially revealing novel transport mechanisms assisted by non-local dissipation. Our platform also offers the prospect of studying quantum information scrambling in purely dissipative cavity QED simulators, complementing prior work on scrambling in unitary simulators [31].

Finally, the ability to squeeze the system at desired wavevectors may be useful for spatially-resolved magnetometry, with the non-local dissipation profile $f_{n,m}$ chosen to optimize sensitivity to a field pattern of interest. Furthermore, while in this work each spin-1/2 particle in the chain is implemented using a single atom, the general principles developed here would also apply to an array of ensembles of atoms which would provide higher field sensitivity [30].

METHODS

Details of the methods used in this work are given in the Supplementary Information where we: (S1) give an explicit experimental construction of a non-local dissipator corresponding to a $\hat{L}_n = \hat{S}_n^-$ loss channel

with an arbitrary translationally invariant spatial profile $f_{n,m}$; (S2) extend time-dependent spin-wave theory to Lindblad dynamics and derive equations of motion for any spin-chain whose dynamics is described by a combination of translationally-invariant Hamiltonians and translationally-invariant Lindblad channels; (S3) further analyze the dynamics of long-range and short-range dissipation from the $\hat{L}_n = \hat{S}_n^-$ loss channel discussed in this work.

ACKNOWLEDGEMENTS

We thank G. Bentsen, P. Calabrese, E. Demler, M. Schleier-Smith, and S. Zeytinoğlu for stimulating discussions. K.S. conducted this research with Government support under and awarded by DoD, Air Force Office of Scientific Research, National Defense Science and Engineering Graduate (NDSEG) Fellowship, 32 CFR 168a. J.M. was supported by the European Union’s Horizon 2020 research and innovation programme under the Marie Skłodowska-Curie grant agreement No 745608 (QUAKE4PRELIMAT), and by the Deutsche Forschungsgemeinschaft (DFG, German Research Foundation) – Project-ID 429529648 – TRR 306 QuCoLiMa (“Quantum Cooperativity of Light and Matter”). A.L. acknowledges funding by the Swiss National Science Foundation. R.F. acknowledges partial financial support from the Google Quantum Research Award. R.F.’s work has been conducted within the framework of the Trieste Institute for Theoretical Quantum Technologies (TQT).

AUTHOR CONTRIBUTIONS

K.S. carried out the analytical calculations and numerics, and discovered the controllability of correlation patterns. K.S. and J.M. prepared the manuscript, and all authors contributed to improving the presentation of results. J.M. and R.F. motivated the examination of non-local dissipation. A.L. provided technical support in developing the time-dependent spin-wave theory for the model. E.J.D helped clarify aspects of the quantum optics implementation. R.F. motivated the search for quantum limit cycles. J.M. oversaw the development of the project.

MATERIALS & CORRESPONDENCE

Supplementary Information is available for this paper. Correspondence and requests for materials should be addressed to Kushal Seetharam (kis@mit.edu).

[1] M. Cheneau, P. Barmettler, D. Poletti, M. Endres, P. Schauß, T. Fukuhara, C. Gross, I. Bloch, C. Kollath, and S. Kuhr, *Nature* **481**, 484 (2012).

[2] P. Calabrese and J. Cardy, *Phys. Rev. Lett.* **96**, 136801 (2006).

[3] R. Islam, R. Ma, P. M. Preiss, M. E. Tai, A. Lukin, M. Rispoli, and M. Greiner, *Nature* **528**, 77 (2015).

[4] S. Diehl, A. Micheli, A. Kantian, B. Kraus, H. Büchler, and P. Zoller, *Nature Physics* **4**, 878 (2008).

[5] F. Verstraete, M. M. Wolf, and J. I. Cirac, *Nature physics* **5**, 633 (2009).

[6] S. Diehl, E. Rico, M. A. Baranov, and P. Zoller, *Nature Physics* **7**, 971 (2011).

[7] M. Höning, M. Moos, and M. Fleischhauer, *Phys. Rev. A* **86**, 013606 (2012).

[8] B. Buča, J. Tindall, and D. Jaksch, *Nat. Comm.* **10**, 1 (2019).

[9] J. T. Barreiro, M. Müller, P. Schindler, D. Nigg, T. Monz, M. Chwalla, M. Hennrich, C. F. Roos, P. Zoller, and R. Blatt, *Nature* **470**, 486 (2011).

[10] Y. Lin, J. Gaebler, F. Reiter, T. R. Tan, R. Bowler, A. Sørensen, D. Leibfried, and D. J. Wineland, *Nature* **504**, 415 (2013).

[11] R. Ma, B. Saxberg, C. Owens, N. Leung, Y. Lu, J. Simon, and D. I. Schuster, *Nature* **566**, 51 (2019).

[12] B. Olmos, D. Yu, and I. Lesanovsky, *Phys. Rev. A* **89**, 023616 (2014).

[13] C. Parmee and N. Cooper, *Physical Review A* **97**, 053616 (2018).

[14] S. Morrison and A. Parkins, *Physical review letters* **100**, 040403 (2008).

[15] A. S. Sørensen and K. Mølmer, *Phys. Rev. A* **66**, 022314 (2002).

[16] H. Krauter, C. A. Muschik, K. Jensen, W. Wasilewski, J. M. Petersen, J. I. Cirac, and E. S. Polzik, *Phys. Rev. Lett.* **107**, 080503 (2011).

[17] E. G. Dalla Torre, J. Otterbach, E. Demler, V. Vuletic, and M. D. Lukin, *Phys. Rev. Lett.* **110**, 120402 (2013).

[18] M. J. Kastoryano, F. Reiter, and A. S. Sørensen, *Phys. Rev. Lett.* **106**, 090502 (2011).

[19] G. Bentsen, T. Hashizume, A. S. Buyskikh, E. J. Davis, A. J. Daley, S. S. Gubser, and M. Schleier-Smith, *Phys. Rev. Lett.* **123**, 130601 (2019).

[20] C.-L. Hung, A. González-Tudela, J. I. Cirac, and H. Kimble, *Proceedings of the National Academy of Sciences* **113**, E4946 (2016).

[21] J. Ma, X. Wang, C.-P. Sun, and F. Nori, *Physics Reports* **509**, 89 (2011).

[22] M. Kormos, M. Collura, G. Takács, and P. Calabrese, *Nature Physics* **13**, 246 (2017).

[23] F. Liu, R. Lundgren, P. Titum, G. Pagano, J. Zhang, C. Monroe, and A. V. Gorshkov, *Phys. Rev. Lett.* **122**, 150601 (2019).

[24] W. Tan, P. Becker, F. Liu, G. Pagano, K. Collins, A. De, L. Feng, H. Kaplan, A. Kyprianidis, R. Lundgren, *et al.*, arXiv preprint arXiv:1912.11117 (2019).

[25] A. Lerose, J. Marino, B. Zunkovic, A. Gambassi, and A. Silva, *Phys. Rev. Lett.* **120**, 130603 (2018).

[26] F. Iemini, A. Russomanno, J. Keeling, M. Schirò, M. Dalmonte, and R. Fazio, *Phys. Rev. Lett.* **121**, 035301 (2018).

[27] M. Oberthaler, private communication.

[28] Z. Zhang, K.-X. Yao, L. Feng, J. Hu, and C. Chin, *Nature Physics* **16**, 652 (2020).

[29] R. M. Kroese, Y. Guo, V. D. Vaidya, J. Keeling, and B. L. Lev, *Phys. Rev. Lett.* **121**, 163601 (2018).

[30] E. J. Davis, A. Periwal, E. S. Cooper, G. Bentsen, S. J. Evered, K. Van Kirk, and M. H. Schleier-Smith, *Phys. Rev. Lett.* **125**, 060402 (2020).

[31] G. Bentsen, I.-D. Potirniche, V. B. Bulchandani, T. Scaffidi, X. Cao, X.-L. Qi, M. Schleier-Smith, and E. Altman, *Phys. Rev. X* **9**, 041011 (2019).

[32] E. J. Davis, G. Bentsen, L. Homeier, T. Li, and M. H. Schleier-Smith, *Phys. Rev. Lett.* **122**, 010405 (2019); E. J. Davis, A. Periwal, E. S. Cooper, Gregory Bentsen, S. J. Evered, K. Van Kirk, and M. H. Schleier-Smith, *Phys. Rev. Lett.* **125**, 060402 (2020).

[33] C.-L. Hung, A. González-Tudela, J. I. Cirac, and H. Kimble, *PNAS* **113**, E4946 (2016).

[34] G. Bentsen, T. Hashizume, A. S. Buyskikh, E. J. Davis, A. J. Daley, S. S. Gubser, and M. Schleier-Smith, *Phys. Rev. Lett.* **123**, 130601 (2019).

[35] G. S. Agarwal, R. R. Puri, and R. P. Singh, *Phys. Rev. A* **56**, 2249 (1997).

[36] A. Sørensen, K. Mølmer, *Phys. Rev. A*, **66**, 022314 (2002).

[37] A. Lerose, B. Zunkovic, J. Marino, A. Gambassi, and A. Silva, *Phys. Rev. B* **99**, 045128 (2019).

[38] A. Lerose, J. Marino, A. Gambassi, and A. Silva, *Phys. Rev. B* **104**306 (2019).

[39] B. Zhu, J. Marino, N. Y. Yao, M. D. Lukin, and E. A. Demler, *New Journal of Physics* **21**, 073028 (2019).

[40] A. Altland and B. Simons, *Condensed Matter Field Theory*, 2nd ed. (Cambridge University Press, Cambridge, 2010).

[41] M. Kastner, *Phys. Rev. Lett.* **106**, 130601 (2011); A. S. Buyskikh, M. Fagotti, J. Schachenmayer, F. Essler, and A. J. Daley, *Phys. Rev. A* **93**, 053620 (2016); A. Campa, T. Dauxois, and S. Ruffo, *Physics Reports* **480**, pp. 57-159 (2009).

[42] A. Lerose and S. Pappalardi, *Phys. Rev. Research* **2**, 012041 (2020).

[43] J. Ma, X. Wang, C.-P. Sun, and F. Nori, *Physics Reports* **509**, 89 (2011).

[44] P. Hauke and L. Tagliacozzo, *Phys. Rev. Lett.* **111**, 207202 (2013); Z.-X. Gong, M. Foss-Feig, S. Michalakis, and A. V. Gorshkov, *Phys. Rev. Lett.* **113**, 030602 (2014). M. Foss-Feig, Z.-X. Gong, C. W. Clark, and A. V. Gorshkov, *Phys. Rev. Lett.* **114**, 157201 (2015); D. V. Else, F. Machado, C. Nayak, and N. Y. Yao, *Phys. Rev. A* **101**, 022333 (2020); M. C. Tran, C.-F. Chen, A. Ehrenberg, A. Y. Guo, A. Deshpande, Y. Hong, Z.-X. Gong, A. V. Gorshkov, and A. Lucas, *Phys. Rev. X* **10**, 031009 (2020)

SUPPLEMENTARY INFORMATION

S1. EXPERIMENTAL CONSTRUCTION

In this section, we give an experimental construction of a non-local dissipator corresponding to a $\hat{L}_n = \hat{S}_n^-$ loss channel with a translationally invariant spatial profile $f(|n - m|)$, as described in Eq. (1) of the main text. Our proposal is motivated by experiments employing clouds of ^{87}Rb atoms coupled to a single photon mode in an optical cavity. In previous works, the cavity mode can be employed as a resource to mediate spin-exchange coherent interactions among the atoms [32], which can be accompanied by collective dissipation depending on the cooperativity of the cavity. Here we work in a complementary limit and engineer incoherent spin emission with spatial resolution. The premise of our construction is to take a chain of atoms, each with three hyperfine levels out of which two are degenerate, trap them inside an optical cavity, and then apply a magnetic field gradient and a Raman beam to the system with several sidebands of tunable frequency and amplitude (see Ref. [33] for a related implementation in photonic waveguides). The magnetic field gradient splits the degeneracy of each atom such that its energy levels form a Λ -configuration; the energies are site-dependent and make the atoms spatially distinct. The Raman beam couples one leg of the Λ -configuration, while the cavity mode couples the other, as shown in Fig. S1(b). The cavity mode mediates communication between atoms at different sites, allowing for both coherent atom-atom interactions as well as indistinguishable atomic losses. The choice of frequencies and amplitudes of the sidebands comprising the Raman beam dictates the probability that atoms at different sites communicate with each other through the cavity photon, thereby setting the spatial profile which shapes both coherent interactions and losses. If the cavity is made to be sufficiently leaky, the coherent interactions are washed out and only dissipative dynamics with the desired spatial profile remains.

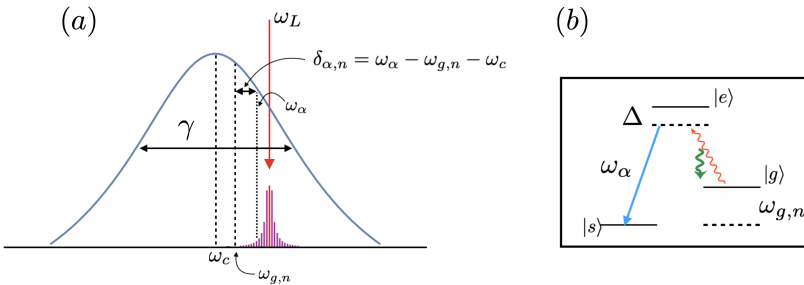


Figure S1. **Schematics of energy scales and detunings.** (a) The cavity mode has frequency ω_c and linewidth γ . For illustrative purposes, we draw the frequency of one of the sidebands, ω_α , which together with the space-dependent energy splitting, $\omega_{g,n}$, of each atom, defines the detunings $\delta_{\alpha,n} \equiv \omega_\alpha - \omega_{g,n} - \omega_c$, for each sideband α and atomic position n . The main carrier frequency of the Raman beam is ω_L , which can typically be set equal to the cavity frequency, ω_c ; purple lines represent the drive amplitudes of each sideband. (b) One of the two Raman processes necessary to engineer non-local losses.

A. Non-local losses

We now give a detailed construction of the experimental implementation. We consider a one-dimensional chain of N atoms labeled by lattice index $n = 1, \dots, N$. Each atom has two internal states $|\tilde{g}\rangle_n$ and $|e\rangle_n$. The state $|\tilde{g}\rangle_n$ belongs to a degenerate hyperfine manifold which, under application of an external field, splits as $|\tilde{g}\rangle_n \rightarrow \{|s\rangle_n, |g\rangle_n\}$. We encode the spin 1/2 Hilbert space $\{|\uparrow\rangle_n, |\downarrow\rangle_n\}$ in this ground state manifold. We take $|s\rangle_n$ to be the lower energy state and set its energy to zero without loss of generality. The energy difference between $|s\rangle_n$ and $|g\rangle_n$ is given as $\omega_{g,n}$ and we will refer to the energy difference between $|s\rangle_n$ and $|e\rangle_n$ as $\omega_{e,n}$. These energies are position dependent since they inherit spatial dependence from the external applied magnetic field gradient. In terms of the operators $\hat{\sigma}_{ab}^n = |a\rangle_n \langle b|_n$, with $a, b \in \{s, g, e\}$, the bare atomic Hamiltonian reads

$$\hat{H}_a = \sum_n (\omega_{e,n} \hat{\sigma}_{ee}^n + \omega_{g,n} \hat{\sigma}_{gg}^n). \quad (\text{S.1})$$

We now dipole-couple the states $|s\rangle_n$ and $|e\rangle_n$ using a Raman driving field $\tilde{\Omega}(t) = \sum_{\alpha=0}^{m_p-1} \Omega_\alpha e^{i\omega_\alpha t}$ where ω_α represents each of the m_p different drive frequencies and Ω_α represents the Rabi frequency (beam amplitude) associated with those frequencies. We can define the frequency $\omega_L \equiv \omega_{\alpha=0}$ as the main frequency and rewrite the driving field in

terms of the detunings $\tilde{\omega}_\alpha \equiv \omega_\alpha - \omega_L$ as $\tilde{\Omega}(t) = \Omega(t) e^{i\omega_L t}$ where $\Omega(t) \equiv \sum_{\alpha=0}^{m_p-1} \Omega_\alpha e^{i\tilde{\omega}_\alpha t}$. Note that $\tilde{\omega}_\alpha = 0$ by definition. The dipole coupling between $|s\rangle_n$ and $|e\rangle_n$ is then described by the Hamiltonian

$$\hat{H}_d = \sum_n \left(\frac{\Omega(t)}{2} e^{i\omega_L t} \hat{\sigma}_{se}^n + \frac{\Omega^*(t)}{2} e^{-i\omega_L t} \hat{\sigma}_{es}^n \right). \quad (\text{S.2})$$

We now consider an optical cavity mode that dipole couples $|g\rangle_n$ and $|e\rangle_n$. The photon mode, represented by the operator \hat{a} , has a frequency ω_c and couples to atom n through the single-photon coupling g . The bare photon Hamiltonian and the light-matter coupling between atoms and photons are given respectively by

$$\hat{H}_p = \omega_c \hat{a}^\dagger \hat{a}, \quad (\text{S.3})$$

$$\hat{H}_{lm} = \sum_n (g \hat{a} \hat{\sigma}_{eg}^n + g^* \hat{a}^\dagger \hat{\sigma}_{ge}^n). \quad (\text{S.4})$$

The total density matrix of the system has dynamics given by the quantum master equation in Lindblad form

$$\frac{d}{dt} \rho = -i [\hat{H}, \rho] + \mathcal{D}_{\text{leak}}(\rho). \quad (\text{S.5})$$

The last term is the dissipator corresponding to photon losses occurring with rate γ

$$\mathcal{D}_{\text{leak}}(\rho) = \gamma \left(\hat{a}^\dagger \rho \hat{a} - \frac{1}{2} \{ \hat{a} \hat{a}^\dagger, \rho \} \right). \quad (\text{S.6})$$

When the excited state $|e\rangle$ is largely detuned by $\Delta = |\omega_e - \omega_L|$ from the other atomic and photonic energy scales ($\Delta \gg \Omega_\alpha, g$), one can use a Schrieffer-Wolf transformation to eliminate the state and write an effective Hamiltonian for the remaining atomic Hilbert space. The light-matter interaction coupling at leading order in $1/\Delta$ then becomes

$$\hat{H}_{lm} = - \sum_n \left(\frac{g\Omega(t)}{\Delta} \hat{a} \hat{\sigma}_{sg}^n e^{i(\omega_L - \omega_c - \omega_{g,n})t} + \frac{g^*\Omega^*(t)}{\Delta} \hat{a}^\dagger \hat{\sigma}_{gs}^n e^{-i(\omega_L - \omega_c - \omega_{g,n})t} \right). \quad (\text{S.7})$$

Defining, $\eta_\alpha \equiv \frac{\Omega_\alpha g}{\Delta}$ and $\delta_{\alpha,n} \equiv \omega_\alpha - \omega_{g,n} - \omega_c$, the interaction Hamiltonian can be written as

$$\hat{H}_{lm} = - \sum_{n,\alpha} [\eta_\alpha \hat{a} \hat{\sigma}_{sg}^n e^{i\delta_{\alpha,n} t} + h.c.]. \quad (\text{S.8})$$

The cavity mode mediates communication between atoms. We now assume that the cavity photon loss is large enough that

$$\gamma \gg \eta_\alpha, \quad \gamma \gg \delta_{\alpha,n}, \quad (\text{S.9})$$

and therefore the cavity photon loss occurs on a timescale much faster than the effective dynamics of the spins. The light field can then be adiabatically eliminated and becomes enslaved to atomic operators [35]. The Heisenberg evolution of the light field can then be expanded in powers of ϵ , with $\epsilon = \eta_\alpha/\gamma$ or $\epsilon = \delta_{\alpha,n}/\gamma$:

$$\hat{a}(t) = i2 \sum_{n,\alpha} \left(\frac{\eta_\alpha^*}{\gamma} \hat{\sigma}_{gs}^n e^{-i\delta_{\alpha,n} t} \right) + 2 \sum_{n,\alpha} \left(\frac{\delta_{\alpha,n} \eta_\alpha^*}{\gamma^2} \hat{\sigma}_{gs}^n e^{-i\delta_{\alpha,n} t} \right) + \mathcal{O}(\epsilon^3), \quad (\text{S.10})$$

Before using the above expression to replace the light field in the full Lindblad equation, Eq. (S.5), we can gain insight into the effective dynamics of the system after elimination of the light field by performing this substitution for the equation of motion of a single spin operator:

$$\begin{aligned} \frac{d}{dt} \hat{\sigma}_{gs}^n &= i \hat{a} \hat{\sigma}_z^n \sum_\alpha \eta_\alpha e^{i\delta_{\alpha,n} t} \\ &\rightarrow -\hat{\sigma}_z^n \sum_{m,\alpha,\beta} (\gamma_{\text{eff}})_{\alpha,\beta} \left(1 - i \frac{\delta_{\beta,m}}{\gamma} \right) e^{i(\delta_{\alpha,n} - \delta_{\beta,m})t} \hat{\sigma}_{gs}^m + \mathcal{O}(\epsilon^3), \end{aligned} \quad (\text{S.11})$$

where we have defined $(\gamma_{\text{eff}})_{\alpha,\beta} \equiv 2\eta_{\alpha}^*\eta_{\beta}/\gamma$. We see that the motion of the n^{th} atom is conditioned by the motion of the m^{th} one, with $(\gamma_{\text{eff}})_{\alpha,\beta}$ setting the effective coupling rate. The leading order contribution to the motion is dissipative dynamics with rate $(\gamma_{\text{eff}})_{\alpha,\beta}$, with the subleading contribution being coherent dynamics with frequency $(\gamma_{\text{eff}})_{\alpha,\beta} \frac{\delta_{\beta,m}}{\gamma}$. When the effective coupling constant, $(\gamma_{\text{eff}})_{\alpha,\beta}$, is much smaller than the minimum detuning between the atomic transition frequencies, we can ignore the off-resonant couplings and only consider the interaction between atoms n and m for which $\delta_{\alpha,n} - \delta_{\beta,m} = 0$. Specifically, we require

$$(\gamma_{\text{eff}})_{\alpha,\beta} \ll \min\{\delta_{\alpha,n} - \delta_{\beta,m}\}, \quad (\text{S.12})$$

where the minimization means the smallest nonzero value of $\delta_{\alpha,n} - \delta_{\beta,m}$. Formally, Eq. (S.12) is derived by taking the long time average of (S.11), and then applying the Sokhotski–Plemelj lemma to extract the singular part of the time integral (resonant process) and the regular part (off-resonant processes). The contribution of the off-resonant term becomes negligible when the condition (S.12) is satisfied (see Ref. [33]). We can then safely restrict the dynamics to the resonance shell $\delta_{\alpha,n} = \delta_{\beta,m}$, which can be restated as

$$\omega_{g,m} - \omega_{g,n} = \tilde{\omega}_{\beta} - \tilde{\omega}_{\alpha}. \quad (\text{S.13})$$

In order to introduce spatial addressability in the system, we choose the site-dependent energy shifts as $\omega_{g,n} = \mu n$, which is implemented via an externally imposed linear magnetic field. We also choose the sideband detunings as $\tilde{\omega}_{\alpha} = \mu \alpha$. After our choice of sideband detunings, the resonance condition Eq. (S.13) reads

$$(\alpha - \beta) = (n - m). \quad (\text{S.14})$$

This selection rule makes pairs of atoms at distance $n - m$ apart interact. The dynamics of a single spin, given by Eq. S.11, then becomes

$$\frac{d}{dt} \hat{\sigma}_{gs}^n \approx -\hat{\sigma}_z^n \sum_{m,\beta} (\gamma_{\text{eff}})_{\beta+(n-m),\beta} \left(1 - i \frac{\delta_{\beta,m}}{\gamma} \right) \hat{\sigma}_{gs}^m, \quad (\text{S.15})$$

and we see that the effective coupling rate, $(\gamma_{\text{eff}})_{\beta+(n-m),\beta}$, depends only on the distance between atoms n and m . The leading order term, corresponding to dissipative dynamics, is therefore translationally invariant. The subleading coherent term, proportional to $\delta_{\beta,m}/\gamma$, however, does have explicit position dependence. We note that if the condition in Eq. (S.12) is violated, then atoms on multiple sites can communicate and even the dissipative dynamics will not be translationally invariant.

We now perform this same adiabatic elimination of the cavity photon on the full Lindblad equation, Eq. (S.5), by replacing \hat{a} with the expression in Eq. (S.10). Keeping terms up to $\mathcal{O}(\epsilon^2)$ in Eq. (S.10), the dissipator given by Eq. (S.6) becomes

$$\mathcal{D}_{\text{leak}}(\rho) \approx 2 \sum_{n,m,\alpha,\beta} (\gamma_{\text{eff}})_{\alpha,\beta} \left(1 + i \frac{(\delta_{\alpha,n} - \delta_{\beta,m})}{\gamma} \right) e^{i(\delta_{\alpha,n} - \delta_{\beta,m})t} \left(\hat{\sigma}_{gs}^m \rho \hat{\sigma}_{sg}^n - \frac{1}{2} \{ \hat{\sigma}_{sg}^n \hat{\sigma}_{gs}^m, \rho \} \right), \quad (\text{S.16})$$

while the coherent light-matter interaction, given by Eq. (S.8), becomes

$$\hat{H}_{\text{lm}} \approx -i2 \sum_{n,m,\alpha,\beta} (\gamma_{\text{eff}})_{\alpha,\beta} e^{i(\delta_{\alpha,n} - \delta_{\beta,m})t} (\hat{\sigma}_{sg}^n \hat{\sigma}_{gs}^m - \hat{\sigma}_{sg}^m \hat{\sigma}_{gs}^n) - 2 \sum_{n,m,\alpha,\beta} (\gamma_{\text{eff}})_{\alpha,\beta} \frac{\delta_{\beta,m}}{\gamma} e^{i(\delta_{\alpha,n} - \delta_{\beta,m})t} \hat{\sigma}_{sg}^n \hat{\sigma}_{gs}^m. \quad (\text{S.17})$$

We see that the first term in the above equation vanishes and we are left with

$$\hat{H}_{\text{lm}} \approx -2 \sum_{n,m,\alpha,\beta} (\gamma_{\text{eff}})_{\alpha,\beta} \frac{\delta_{\beta,m}}{\gamma} e^{i(\delta_{\alpha,n} - \delta_{\beta,m})t} \hat{\sigma}_{sg}^n \hat{\sigma}_{gs}^m. \quad (\text{S.18})$$

The master equation for the density matrix describing the system can thus be written as

$$\frac{d}{dt} \rho \approx 2 \sum_{n,m,\alpha,\beta} (\gamma_{\text{eff}})_{\alpha,\beta} \left(1 + i \frac{(\delta_{\alpha,n} - \delta_{\beta,m})}{\gamma} \right) e^{i(\delta_{\alpha,n} - \delta_{\beta,m})t} \left(\hat{\sigma}_{gs}^m \rho \hat{\sigma}_{sg}^n - \frac{1}{2} \{ \hat{\sigma}_{sg}^n \hat{\sigma}_{gs}^m, \rho \} \right) + \quad (\text{S.19})$$

$$+ i2 \sum_{n,m,\alpha,\beta} (\gamma_{\text{eff}})_{\alpha,\beta} \frac{\delta_{\beta,m}}{\gamma} e^{i(\delta_{\alpha,n} - \delta_{\beta,m})t} [\hat{\sigma}_{sg}^n \hat{\sigma}_{gs}^m, \rho]. \quad (\text{S.20})$$

If the condition Eq. (S.12) is satisfied, then we can restrict dynamics to the resonance shell defined by Eq. (S.13) and the resulting Lindblad equation is

$$\frac{d}{dt}\rho \approx \left(\frac{4|g|^2\Omega_M^2}{\gamma\Delta^2}\right) \sum_{n,m} f_{n,m} \left(\hat{\sigma}_{gs}^m \rho \hat{\sigma}_{sg}^n - \frac{1}{2} \{ \hat{\sigma}_{sg}^n \hat{\sigma}_{gs}^m, \rho \} \right) + i \left(\frac{4|g|^2\Omega_M^2}{\gamma\Delta^2}\right) \sum_{n,m} \left[\tilde{f}_{n,m} \hat{\sigma}_{sg}^n \hat{\sigma}_{gs}^m, \rho \right] \quad (\text{S.21})$$

where

$$f_{n,m} = \sum_{(\alpha,\beta);(\alpha-\beta)=(n-m)} \frac{\Omega_\alpha \Omega_\beta^*}{\Omega_M^2}, \quad \tilde{f}_{n,m} = \sum_{(\alpha,\beta);(\alpha-\beta)=(n-m)} \frac{\delta_{\beta,m}}{\gamma} \frac{\Omega_\alpha \Omega_\beta^*}{\Omega_M^2}. \quad (\text{S.22})$$

In the above equation, we define Ω_M as the largest Raman sideband amplitude and choose it as a representative scale for the drive. Note that the term in Eq. (S.19) that is proportional to $\delta_{\alpha,n}$ exactly cancels the term proportional to $\delta_{\beta,m}$ when we satisfy the two-atom resonance condition Eq. (S.13).

Collating the conditions, Eq. (S.9) and Eq. (S.12), for adiabatically eliminating the cavity photon, we have:

$$\eta_\alpha \ll \gamma, \quad \delta_{\alpha,n} \ll \gamma, \quad \frac{\eta_\alpha \eta_\beta^*}{\min\{\delta_{\alpha,n} - \delta_{\beta,m}\}} \ll \gamma. \quad (\text{S.23})$$

Recall that in the third condition above, the denominator, $\min\{\delta_{\alpha,n} - \delta_{\beta,m}\}$, is a minimization over processes with $\delta_{\alpha,n} \neq \delta_{\beta,m}$. For any fixed η_α and $\delta_{\alpha,n}$, a sufficiently large cavity decay γ allows all three conditions to be simultaneously satisfied. Later, we show that these conditions can be consistently satisfied by providing numerical estimates using parameters from cavity QED experiments. We note that the condition $\delta_{\alpha,n} \ll \gamma$ is satisfied by choosing a large cavity decay, γ , and a non-zero $\delta_{\alpha,n}$. In fact, we require that $\delta_{\alpha,n} \neq 0$ in order to preserve spatial structure in the dynamics. We can see this by setting $\delta_{\alpha,n} = 0$ in Eq. (S.10) to get $\hat{a}(t) = i\zeta \hat{\sigma}_{gs}$ where $\hat{\sigma}_{gs} = \sum_n \hat{\sigma}_{gs}^n$ and $\zeta = \frac{2}{\gamma} \sum_\alpha \eta_\alpha^*$. Single-atom resonant processes, characterized by $\delta_{\alpha,n} = 0$, therefore only lead to collective dissipation of all spins in the system, arising from collective emission of the cavity photon, rather than non-local dissipation with spatial structure.

Physically, we can interpret the set-up resulting in Eq. (S.21) as follows. Both non-local dissipation and coherent interactions amongst the spins are mediated by non-resonant virtual photons, corresponding to $\delta_{\alpha,n} \neq 0$, which satisfy the two-atom resonance condition $\delta_{\alpha,n} = \delta_{\beta,m}$. The spatial profile of the resulting non-local dissipation, $f_{n,m}$, is translationally invariant and represents leakage of a cavity photon without certainty about which of the two atoms, n or m , it came from. The spatial profile of the coherent interaction, $\tilde{f}_{n,m}$, represents a spin-exchange between the atoms which is suppressed by a factor $\delta_{\beta,m}/\gamma$ due to the highly lossy cavity. The conditions in Eq. (S.23) represent a regime where the cavity loss, γ , is large enough that: (i) the effective dynamics of each individual spin, occurring through a Λ -process in the atom with rate η_α , occurs slowly compared to the cavity photon loss so the photon only serves to mediate coherent interactions and non-local emission from pairs of spins, (ii) coherent interactions of the spins are suppressed, and (iii) the time-scale of the effective non-local emission from pairs of spins, set by $\tau = 1/(\gamma_{\text{eff}})_{\alpha,\beta} \propto \gamma/\eta_\alpha^* \eta_\beta$, is slow enough that off-resonant two-atom processes ($\delta_{\alpha,n} \neq \delta_{\beta,m}$) average to zero and only the resonant two-atom process remains. This resonant two-atom process is a translationally-invariant non-local emission from pairs of atoms.

The quantity $f_{n,m} = f(|n-m|)$ only depends on the difference $n-m$ and sets the spatial profile of the non-local dissipation. We can design the desired translationally-invariant profile $f_{n,m} = f(|n-m|)$ of the dissipator by exactly solving $f(|n-m|) = \sum_{(\alpha,\beta);(\alpha-\beta)=(n-m)} \Omega_\alpha \Omega_\beta^* / \Omega_M^2$. Later, we explicitly show how to numerically invert this equation. Defining $\kappa = |g|^2 \Omega_M^2 / (\gamma \Delta^2)$ and relabeling the projection operators as $\hat{S}_n^- = \hat{\sigma}_{gs}^n / 2$ and $\hat{S}_n^+ = \hat{\sigma}_{sg}^n / 2$, we have

$$\frac{d}{dt}\rho \approx \kappa \sum_{n,m} f(|n-m|) \left(\hat{S}_m^- \rho \hat{S}_n^+ - \frac{1}{2} \{ \hat{S}_n^+ \hat{S}_m^-, \rho \} \right) + i \left[\kappa \sum_{n,m} \tilde{f}_{n,m} \hat{S}_n^- \hat{S}_m^+, \rho \right] \quad (\text{S.24})$$

The first term in Eq. (S.24) is the desired non-local dissipation while the second term represents coherent spin-exchange interactions mediated by a virtual photon emitted in the Λ -process within one atom and absorbed via the reverse Λ -process in a second atom a distance $|n-m|$ away [33, 34]. Comparing the expressions for $\tilde{f}_{n,m}$ and $f_{n,m}$ in Eq. (S.22), we see that the coherent dynamics are subleading to the dissipative dynamics. Therefore, when the cavity decay is large enough that $\gamma \gg \delta_{\beta,m}$, the coherent dynamics vanishes and we are left with purely dissipative dynamics with a spatial profile $f(|n-m|)$:

$$\frac{d}{dt}\rho = \kappa \sum_{n,m} f(|n-m|) \left(\hat{S}_n^- \rho \hat{S}_m^+ - \frac{1}{2} \{ \hat{S}_m^+ \hat{S}_n^-, \rho \} \right) \quad (\text{S.25})$$

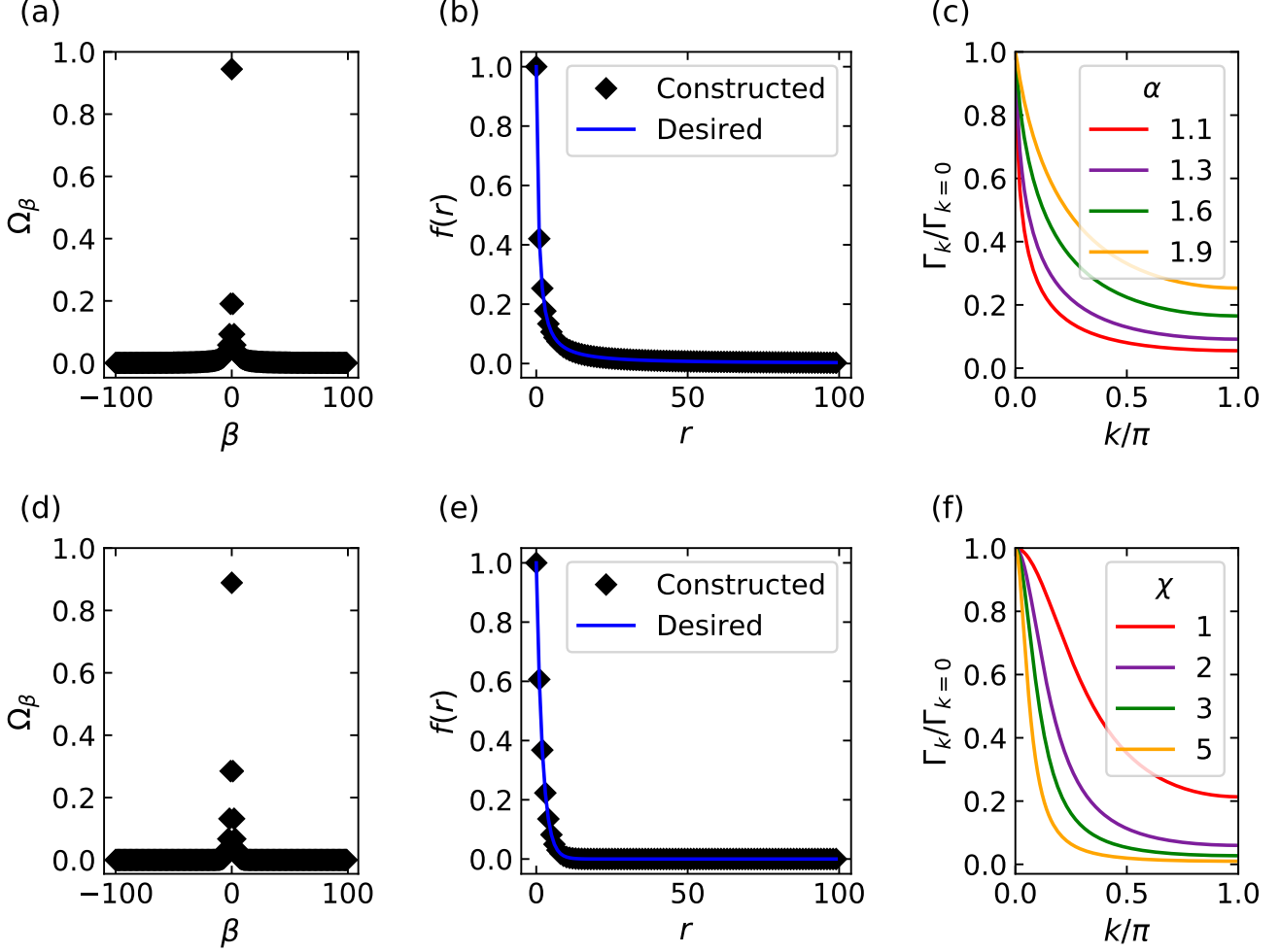


Figure S2. **Sideband amplitude construction.** (a) Sideband amplitudes required to construct a long-range spatial profile $f(|n - m|) = (|n - m| + 1)^{-\alpha}$ on a 100 site chain. (b) Spatial profile resulting from the amplitudes in (a). (c) Fourier transform of the long-range spatial profile. (d) Sideband amplitudes required to construct a short-range spatial profile $f(|n - m|) = e^{-|n - m|/\chi}$ on a 100 site chain. (e) Spatial profile resulting from the amplitudes in (d). (f) Fourier transform of the short-range spatial profile.

which is the non-local $\hat{L}_n = \hat{S}_n^-$ loss channel we aimed to construct. The positivity of this Lindblad map is guaranteed by the positivity of the Raman sideband amplitudes Ω_β that determine $f(|n - m|)$; we require $f(|n - m| = 0) \neq 0$ to ensure a positive Lindblad map, which is violated only when all sideband amplitudes are zero and we have no dynamics.

B. Engineering the spatial profile

We now show how to construct a desired dissipation profile $f(|n - m|)$ by choosing the Raman sideband amplitudes $\{\Omega_\beta\}$ appropriately. In this section, we work in units where the maximum sideband amplitude is normalized to 1 ($\Omega_M = 1$). The equation we want to invert is

$$\begin{aligned} f(|n - m|) &= \sum_{\alpha, \beta; (\alpha - \beta) = (n - m)} \Omega_\alpha \Omega_\beta^* \\ &= \sum_{\beta} \Omega_{\beta + (n - m)} \Omega_\beta^*, \end{aligned}$$

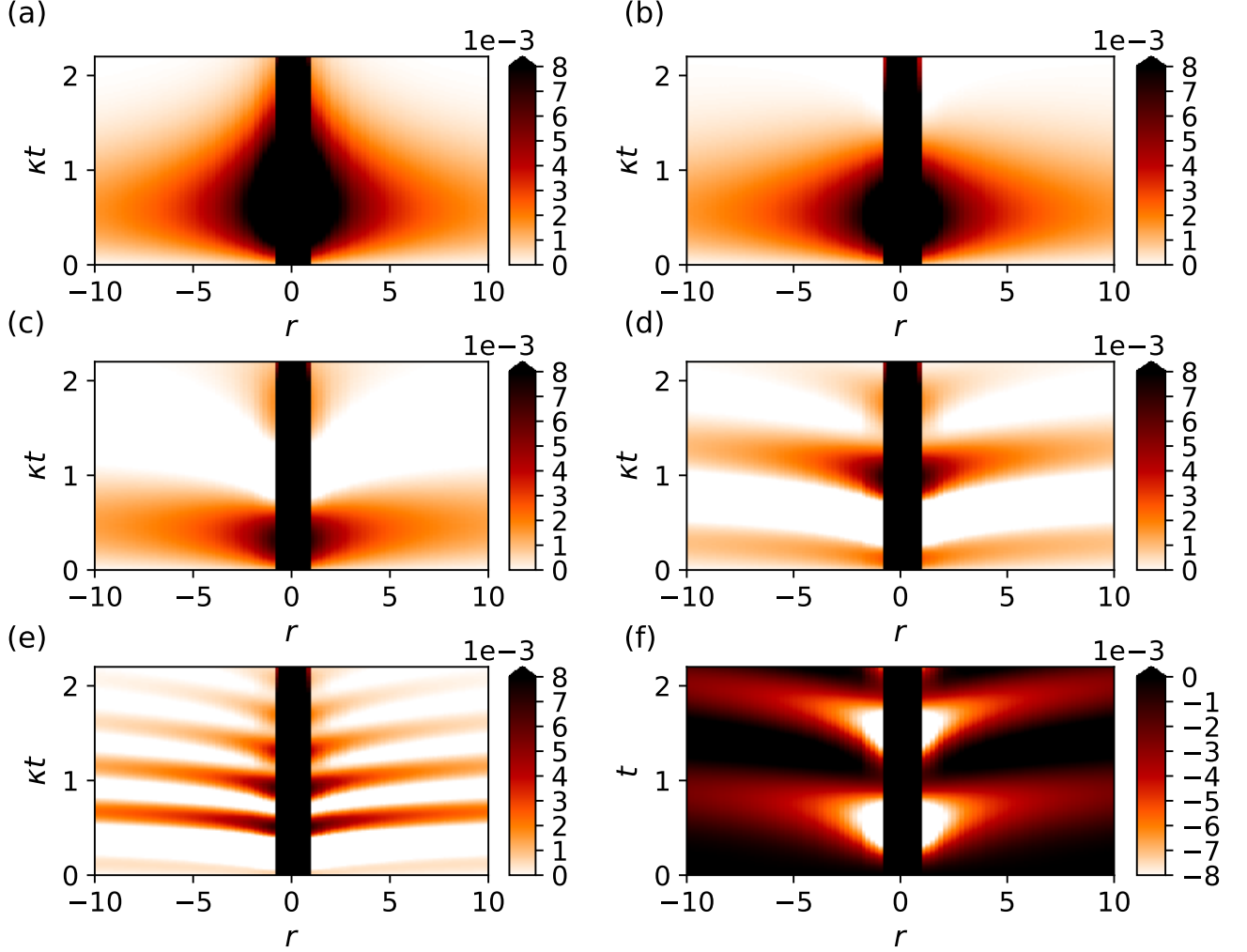


Figure S3. Crossover between dissipative and coherent dynamics. We compute the correlation function $C^{zz}(r, t)$ for a system whose dynamics is comprised of a long-range dissipation channel ($\hat{L}_n = \hat{S}_n^-$) with strength κ and a long-range spin-exchange Hamiltonian with strength η . For both generators, the spatial profile is $f(|n - m|) = (|n - m| + 1)^{-\alpha}$ with $\alpha = 1.25$. The system exhibits a crossover between $\eta/\kappa = 0.25$ and $\eta/\kappa = 0.5$. **a** $\kappa = 1.0$, $\eta = 0.0$ (only dissipation). **b** $\kappa = 1.0$, $\eta = 0.25$. **c** $\kappa = 1.0$, $\eta = 0.5$. **d** $\kappa = 1.0$, $\eta = 1.0$. **e** $\kappa = 1.0$, $\eta = 2.0$. **f** $\kappa = 0.0$, $\eta = 1.0$ (only Hamiltonian).

with $r \equiv n - m$. For a system of N spins, we have $r = -(N - 1), -(N - 2), \dots, 0, \dots, (N - 2), (N - 1)$. Recalling that $f(|n - m|) = f(r)$ is a translationally invariant profile, we have

$$f(r) = \sum_{\beta} \Omega_{\beta+r} \Omega_{\beta}^*, \quad (\text{S.26})$$

where we will need $2N - 1$ sidebands corresponding to the values that r can take; the sidebands $\{\Omega_{\beta}\}$ are indexed as $\beta = -(N - 1), -(N - 2), \dots, 0, \dots, (N - 2), (N - 1)$. Note that Eq. (S.26) shows that the profile $f(r)$ is simply the discrete autocorrelation of the sideband amplitudes. We can thus make use of the convolution theorem to take the discrete Fourier transform (DFT) of both sides:

$$f(k) = |\Omega_k|^2, \quad (\text{S.27})$$

where we define the DFT as $f(k) = \sum_r e^{-ikr} f(r)$ and $\Omega_k = \sum_{\beta} e^{-ik\beta} \Omega_{\beta}$, introducing the inverse DFT as $f(r) = \frac{1}{(2N-1)} \sum_k e^{ikr} f(k)$ and $\Omega_{\beta} = \frac{1}{(2N-1)} \sum_k e^{ik\beta} \Omega_k$. We know that any choice of $f(|n - m|)$ which yields a physically valid dissipator must be positive semidefinite, and therefore $f(k)$ must be real and non-negative. We can take its square root and get

$$|\Omega_k| = \sqrt{f(k)}. \quad (\text{S.28})$$

Now, we can look for solutions with Ω_k real, thus yielding

$$\Omega_\beta = \frac{1}{(2N-1)} \sum_k e^{ik\beta} \sqrt{f(k)} \quad (\text{S.29})$$

which are the desired sideband amplitudes. One can numerically compute these amplitudes using a fast Fourier transform and then check that the amplitudes yield the desired profile by computing their autocorrelation (Eq. (S.26)). In Fig. S2, we demonstrate this procedure for a long-range spatial profile $f(|n-m|) = \frac{1}{(|n-m|+1)^\alpha}$ and a short-range spatial profile $f(|n-m|) = e^{-|n-m|/\chi}$.

C. Parameter estimates for cavity QED experiments

For the construction to hold, we require that the detuning, Δ , and cavity loss rate, γ , are sufficiently large. Specifically, we require that $\Delta \gg \mu N$, $\Delta \gg \omega_L - \omega_c - \omega_{g,n}$, and $\Delta \gg \Omega_M, g$. These conditions result in the excited atomic level $|e\rangle_n$ having approximately the same energy along the entire chain and only participating virtually in the dynamics. We also require that $\gamma \gg g\Omega_M/\Delta$ and $\gamma \gg \delta_{\beta,m}$, which allow us to adiabatically eliminate the photon and suppress coherent spin-exchange interactions respectively. Lastly, we require that $\Delta^2\gamma \gg g^2\Omega_M^2/\min|\omega_{g,n} - \omega_{g,m}|$ so that only the resonant process Eq. (S.13) takes place.

Below we provide estimates for the parameters involved in the experiment of Ref. [32] and show that our construction is accessible to current experimental systems. The number of lattice sites is $N \approx 100$ and it is comparable to the number of sidebands ≈ 50 -100 in the Raman beam. The Raman beam Rabi frequency $|\Omega|$ and cavity mode coupling g range are on the order of a few MHz. The carrier frequency ω_L is ≈ 384 THz, while the sideband frequencies of the Raman beam satisfy $\max\{|\tilde{\omega}_\alpha - \tilde{\omega}_\beta|\} \approx 10$ kHz. The Zeeman splitting $\omega_{g,n} = \mu n$ on each site is given by a magnetic field $\mu \cdot L \approx 500$ kHz, where L is the length of the cloud. Finally, the cavity decay γ is in the range ≈ 200 kHz – 10 of MHz. Per these experimental parameters, we can estimate that $\mu N/\Delta \sim 10^{-5}$, $(\omega_L - \omega_c - \omega_{g,n})/\Delta \sim 10^{-4}$, $\Omega_M/\Delta \sim g/\Delta \sim 10^{-4}$, $\delta_{\beta,m}/\gamma \sim 10^{-1}$, $g\Omega_M/(\Delta\gamma) \sim 10^{-4}$, and $g^2\Omega_M^2/(\min|\omega_{g,n} - \omega_{g,m}| \Delta^2\gamma) \sim 10^{-1}$. The conditions for achieving the desired effective dynamics are thus satisfied.

While we should safely be able to ignore the coherent spin-exchange dynamics described in Eq. S.24, we can further examine the robustness of our platform to subleading effects. In Fig. S3, we plot the correlation dynamics when both dissipative and coherent dynamics are present. As the relative strength of the coherent dynamics is increased, the pattern of correlations demonstrates a cross-over between the dissipative confinement pattern discussed in the main text and correlation fronts characteristic of a purely coherent dynamics arising from a spin-exchange Hamiltonian. The dissipative confinement pattern survives even when the coherent dynamics is one-fourth as strong as the dissipative dynamics; the experimental estimate of $\delta_{\beta,m}/\gamma \sim 10^{-1}$ is well below this threshold.

The subleading spin-exchange Hamiltonian rotates the collective spin similar to a uniform external field and one may consider using it to tune the correlation pattern. However, as the spin-exchange dynamics also inherits a spatial profile, it complicates the spread of correlations and therefore makes an inconvenient tool to engineer a desired pattern arising from the dissipative dynamics. A uniform external field cannot create any spatial correlations, and therefore acts as a simple knob that tunes dynamics arising from the dissipator.

We note that such a uniform external field requires an addition to the experimental construction. It can be implemented, for example, by shining an additional multifrequency Raman beam that directly couples the two lower atomic levels with sideband frequencies corresponding to the change in energy splittings on each site. The amplitude ω_F characterizing the strength of this effective magnetic field would be set by the Rabi frequency Ω_x of this additional Raman beam, which typically takes on values between 1 kHz to 50 kHz in the experiment referenced above.

Lastly, we consider the effect of local losses from spontaneous Raman scattering of the individual atoms into free space. These incoherent spin losses are present in all experiments and introduce undesired decohering effects that deplete the total magnetization of the system. Following Ref. [36], we estimate the number of spontaneous emission events after a time t as $N_\Sigma \simeq N\Sigma t\Omega_M^2/\Delta^2$, with Σ being the decay rate and N being the total number of excitations in the system. The relevant time scale is set by the rate at which non-local dissipation generates correlations, given by $t \sim 1/\kappa \sim \gamma\Delta^2/g^2\Omega_M^2$. Correlations generated on this time scale are preserved if the number of spontaneous emission events is small compared to the number of atoms in the system: we require $N_\Sigma \ll N$. To satisfy this requirement, we need $\Sigma\gamma/g^2 \ll 1$, which together with the above stated condition of leaky cavity $\gamma \gg g\Omega_M/\Delta$, yields $\Sigma \ll (\Delta/\Omega_M)^2\gamma$. In the setup of Ref. [32], we have $\Omega_M/\Delta \sim 10^{-4}$, and as both Σ and γ are typically of the order of a few MHz, correlations generated from non-local dissipation are protected against scattering into free space for a long window of time. We can alternatively combine the conditions $\Sigma\gamma/g^2 \ll 1$ and $\gamma \gg g\Omega_M/\Delta$ into $g \gg \Sigma\Omega_M/\Delta$, which states that the coupling between the atoms and the cavity mode should be strong enough that coherent cavity-mediated transitions between atomic energy levels should be much more frequent than incoherent transitions due to

spontaneous emission. For the parameters of Ref. [32], g and Σ are of the order of a few MHz and $\Omega_M/\Delta \sim 10^{-4}$ so this strong coupling condition is satisfied.

S2. TIME-DEPENDENT SPIN-WAVE THEORY

In this section, we use time-dependent spin-wave theory (TDSW) to derive equations of motion for translationally-invariant spin chains described by a master equation consisting of both unitary and dissipative dynamics. Previously, TDSW has been used to study the non-equilibrium dynamics of a variety of unitary systems including interacting spin chains with competing short and long range interactions [25, 37, 38], as well as interacting spin models coupled to a cavity mode [39]. Here, we extend the method to Lindblad dynamics and derive equations of motion for any system whose dynamics is described by a combination of translationally-invariant Hamiltonians and translationally-invariant Lindblad channels. Our derivation can be used to construct equations of motion for the system described in Eq. (1) of the main text, all unitary systems studied in prior literature, and for any translationally-invariant system whose dynamics is described by a master equation.

The premise of TDSW is to assume that the system is well-described by a time-dependent collective spin with a small number of spin-wave excitations on top of this collective motion. The motion of the collective spin and the spin-waves are coupled. As the number of spin-waves is assumed to be small, we can treat the spins as bosons and the dynamics of the system is reduced to the motion of excitations on top of a moving ‘condensate’. Formally, the treatment is a self-consistent time-dependent Hartree approximation of the lowest order Holstein-Primakoff expansion of the spins. The method is valid when the relevant excitations of the system are spin-waves and during the portion of dynamics in which the spin-wave density remains small. The advantage of TDSW is that it allows us to examine the dynamics of a thermodynamically large number of spins whenever the above two conditions are met. This typically results in control of dynamics over a time window significantly larger than what permissible with conventional low order Holstein-Primakoff expansions [40].

A. Types of channels

We consider translationally-invariant spin systems that are describable by a master equation constructed from a combination of three types of dynamical channels, each characterized by a spin operator of the form

$$\hat{L}_n = c_x \hat{S}_n^x + c_y \hat{S}_n^y + c_z \hat{S}_n^z \quad (\text{S.30})$$

with $\{c_x, c_y, c_z\}$ being arbitrary (complex) coefficients.

The first type of channel is unitary dynamics from a collective field which is generated by the Hamiltonian

$$\hat{H}_F = \omega_F \sum_n \hat{L}_n. \quad (\text{S.31})$$

The second type of channel is unitary dynamics with spatial character generated by a Hamiltonian

$$\hat{H}_L = \frac{\eta}{s\Gamma_{k=0}} \sum_{n,m} f(|n-m|) (\hat{L}_m^\dagger \hat{L}_n + h.c.) \quad (\text{S.32})$$

where $\Gamma_k \equiv \sum_{r \in \{-\frac{N}{2}, \frac{N}{2}\}} e^{ikr} f(|n-m|)$ is the Fourier transform of the spatial profile $f(|n-m|)$, N is the number of spins in the system, and s is the total spin of each spin on the chain (typically taken to be $s = 1/2$). The strength of the channel is defined with a factor of $\Gamma_{k=0}$ as per the usual Kac renormalization that is used to normalize the contribution of this channel to dynamics in the case that $f(|n-m|)$ is long-range [41].

Combinations of the above Hamiltonian can be used to construct most unitary models of interest, including the Heisenberg XYZ model as well as common one-axis and two-axis twisting Hamiltonians.

The third type of channel is dissipative dynamics generated by a jump operator \hat{A}_n . The contribution of this channel to an adjoint master equation for an operator \hat{A} is

$$\mathcal{D}_L(\hat{A}) = \frac{\kappa}{s\Gamma_{k=0}} \sum_{n,m} f(|n-m|) \left(\hat{L}_n^\dagger \hat{A} \hat{L}_m - \frac{1}{2} \{ \hat{L}_m^\dagger \hat{L}_n, \hat{A} \} \right), \quad (\text{S.33})$$

where we have once again renormalized the strength of the channel with $\Gamma_{k=0}$. The usual cases of spatially homogeneous dissipation can be recovered by choosing $f(|n-m|) = \delta_{n,m}$ for individual dissipation and $f(|n-m|) = \text{constant}$

for collective dissipation. Note that the interaction matrix $f(|n - m|)$ for a valid Lindblad map must be positive semi-definite; this condition is violated if the same-site component of the spatial profile $f(|n - m| = 0)$ vanishes. Therefore, a valid dissipative channel will always include a component of independent loss from each site. This requirement is the reason for defining the long-range dissipation profile as $f(|n - m|) = (|n - m| + 1)^{-\alpha}$ rather than $f(|n - m|) = |n - m|^{-\alpha}$ as is usually done for long-range Hamiltonians.

The dynamics of an operator \hat{A} can then be expressed with an adjoint master equation

$$\frac{d}{dt}\hat{A} = \sum_j \frac{1}{i} [\hat{A}, \hat{H}_j] + \sum_{j'} \mathcal{D}_{j'} (\hat{A}) \quad (\text{S.34})$$

where the sums run over Hamiltonians and dissipators of the types described above. As the system is translationally-invariant, we assume periodic boundary conditions and define the Fourier transform of the spin components as $\hat{S}_k^\alpha = \sum_n e^{-ikn} \hat{S}_n^\alpha$ with $\alpha \in \{x, y, z\}$. The inverse transform is given by $\hat{S}_n^\alpha = \frac{1}{N} \sum_k e^{ikn} \hat{S}_k^\alpha$. The spins in Fourier space satisfy the commutation relation $[\hat{S}_k^\alpha, \hat{S}_{k'}^\beta] = i\epsilon^{\alpha\beta\gamma} \hat{S}_{k+k'}^\gamma$.

We now rotate to a time-dependent frame defined by angles $\theta(t)$ and $\phi(t)$. Specifically, we apply the unitary transformation $\hat{V}(\theta, \phi) = e^{-i\phi} \sum_n S_n^z e^{-i\theta} \sum_n S_n^y$. Letting e_α be the unit vectors of the lab frame, the unit vectors of the rotated frame, $e_{\tilde{\alpha}}$, are given as

$$e_{\tilde{x}} = \begin{pmatrix} \cos \theta \cos \phi \\ \cos \theta \sin \phi \\ -\sin \theta \end{pmatrix}, \quad e_{\tilde{y}} = \begin{pmatrix} -\sin \phi \\ \cos \phi \\ 0 \end{pmatrix}, \quad e_{\tilde{z}} = \begin{pmatrix} \sin \theta \cos \phi \\ \sin \theta \sin \phi \\ \cos \theta \end{pmatrix}. \quad (\text{S.35})$$

We will later choose $\theta(t)$ and $\phi(t)$ so that the z-axis of the rotated frame, $e_{\tilde{z}}$, aligns with the z-component of the collective spin $\hat{S}^{\tilde{\alpha}} = \sum_n \hat{S}_n^{\tilde{\alpha}} = \hat{S}_{k=0}^{\tilde{\alpha}}$. The cost of this time-dependent rotation is an additional Hamiltonian

$$\hat{H}_{\text{RF}} = \sin \theta \dot{\phi} \hat{S}^{\tilde{x}} - \dot{\theta} \hat{S}^{\tilde{y}} - \cos \theta \dot{\phi} \hat{S}^{\tilde{z}} \quad (\text{S.36})$$

that contributes to the dynamics. The three types of dynamical channels that contribute to the dynamics of an operator \hat{A} in the rotated frame take the form

$$\hat{H}_F = \omega_F \sum_{\tilde{\alpha} \in \{\tilde{x}, \tilde{y}, \tilde{z}\}} F_{\tilde{\alpha}} \hat{S}_{k=0}^{\tilde{\alpha}} \quad (\text{S.37})$$

$$\hat{H}_L = \frac{2\eta}{\Gamma_{k=0} N s} \sum_k \Gamma_k \sum_{\tilde{\alpha}, \tilde{\beta} \in \{\tilde{x}, \tilde{y}, \tilde{z}\}} M_{\tilde{\alpha}, \tilde{\beta}} \hat{S}_{-k}^{\tilde{\alpha}} \hat{S}_k^{\tilde{\beta}} \quad (\text{S.38})$$

$$\mathcal{D}_L (\hat{A}) = \frac{\kappa}{\Gamma_{k=0} N s} \sum_k \Gamma_k \sum_{\tilde{\alpha}, \tilde{\beta} \in \{\tilde{x}, \tilde{y}, \tilde{z}\}} M_{\tilde{\alpha}, \tilde{\beta}} \left(\hat{S}_k^{\tilde{\alpha}} \hat{A} \hat{S}_{-k}^{\tilde{\beta}} - \frac{1}{2} \left\{ \hat{S}_{-k}^{\tilde{\alpha}} \hat{S}_k^{\tilde{\beta}}, \hat{A} \right\} \right) \quad (\text{S.39})$$

where we have defined

$$F_{\tilde{\alpha}}(\theta, \phi) = c_x G_{\tilde{\alpha}, x} + c_y G_{\tilde{\alpha}, y} + c_z G_{\tilde{\alpha}, z} \quad (\text{S.40})$$

$$M_{\tilde{\alpha}, \tilde{\beta}}(\theta, \phi) = (c_x^* G_{\tilde{\alpha}, x} + c_y^* G_{\tilde{\alpha}, y} + c_z^* G_{\tilde{\alpha}, z}) (c_x G_{\tilde{\beta}, x} + c_y G_{\tilde{\beta}, y} + c_z G_{\tilde{\beta}, z}) \quad (\text{S.41})$$

and $G_{\alpha\beta} = e_{\tilde{\alpha}} \cdot e_\beta$ is the projection of the rotated basis vectors on the lab frame basis vectors. The choice of operator \hat{L}_n is encoded in $F_{\tilde{\alpha}}(\theta, \phi)$ or $M_{\tilde{\alpha}, \tilde{\beta}}(\theta, \phi)$ while the choice of spatial profile $f(|n - m|)$ is encoded in Γ_k . Note that the dynamics of the above channels does not decompose into independent dynamics for each wave vector k as sectors of different momenta are coupled via the self-consistent feedback of the $k = 0$ mode.

B. Low order Holstein-Primakoff expansion in a moving vacuum

We now bosonize the spins via a lowest-order Holstein-Primakoff transformation

$$\hat{S}_n^{\tilde{z}} = s - \hat{b}_n^\dagger \hat{b}_n, \quad \hat{S}_n^+ = (2s)^{\frac{1}{2}} \hat{b}_n, \quad \hat{S}_n^- = (2s)^{\frac{1}{2}} \hat{b}_n^\dagger \quad (\text{S.42})$$

where \hat{b}_n^\dagger and \hat{b}_n are bosonic creation and annihilation operators representing spin flips along the chain and satisfy canonical commutation relations $[\hat{b}_n, \hat{b}_m^\dagger] = \delta_{nm}$. In Fourier space, the mapping becomes

$$\hat{S}_k^{\tilde{x}} = \left(\frac{Ns}{2}\right)^{\frac{1}{2}} \left\{ \hat{b}_k + \hat{b}_k^\dagger \right\}, \quad \hat{S}_k^{\tilde{y}} = \frac{1}{i} \left(\frac{Ns}{2}\right)^{\frac{1}{2}} \left\{ \hat{b}_k - \hat{b}_k^\dagger \right\}, \quad \hat{S}_k^{\tilde{z}} = Ns\delta_{k,0} - \sum_{k'} \hat{b}_{k'}^\dagger \hat{b}_{k+k'} \quad (\text{S.43})$$

where $\hat{b}_k^\dagger = \frac{1}{\sqrt{N}} \sum_n e^{ikn} \hat{b}_n^\dagger$ and $\hat{b}_k = \frac{1}{\sqrt{N}} \sum_n e^{-ikn} \hat{b}_n$ are bosonic creation and annihilation operators representing spin-wave excitations. It is useful to work in terms of quadrature operators \hat{q}_k and \hat{p}_k which are expressed in terms of the creation and annihilation operators as $\hat{b}_k^\dagger = \frac{1}{\sqrt{2}} (\hat{q}_k - i\hat{p}_k)$ and $\hat{b}_k = \frac{1}{\sqrt{2}} (\hat{q}_k + i\hat{p}_k)$. Note that these momentum space quadrature operators satisfy the commutation relation $[\hat{q}_k, \hat{p}_{k'}] = i\delta_{k',-k}$. The mapping between spins and bosonic modes can be given in terms of the quadrature operators as

$$\hat{S}_k^{\tilde{x}} = (Ns)^{\frac{1}{2}} \hat{q}_k, \quad \hat{S}_k^{\tilde{y}} = (Ns)^{\frac{1}{2}} \hat{p}_k, \quad \hat{S}_k^{\tilde{z}} = Ns\delta_{k,0} - \frac{1}{2} \sum_{k'} (\hat{q}_{k'} \hat{q}_{k-k'} + \hat{p}_{k'} \hat{p}_{k-k'} - \delta_{k,0}). \quad (\text{S.44})$$

It is also useful to define

$$n_k = \langle \hat{b}_k^\dagger \hat{b}_k \rangle = \frac{1}{2} \langle (\hat{q}_k \hat{q}_{-k} + \hat{p}_k \hat{p}_{-k} - 1) \rangle \quad (\text{S.45})$$

with $n_{k=0}$ corresponding to the condensate density and $n_{k \neq 0}$ corresponding to the occupation of the spin-wave mode at wavevector k . The evolution of the $k = 0$ mode represents the dynamics of the spin-wave vacuum and the evolution of the $k \neq 0$ represents dynamics of spin-waves on top of the moving vacuum. In the thermodynamic limit, we can treat the spin-wave vacuum classically [42], while treating the spin-waves as quantum mechanical excitations. In practice, this amounts to replacing $\hat{S}_{k=0}^{\tilde{z}}$ by a c-number $\langle \hat{S}_{k=0}^{\tilde{z}} \rangle$ and using the total spin-wave density

$$\epsilon(t) = \frac{1}{Ns} \sum_{k \neq 0} n_k(t) = \frac{1}{Ns} \sum_{k \neq 0} \frac{\langle \hat{q}_k(t) \hat{q}_{-k}(t) + \hat{p}_k(t) \hat{p}_{-k}(t) - 1 \rangle}{2} \quad (\text{S.46})$$

as a control parameter for the approximation. As long as $\epsilon(t)$ remains small, the majority of angular momentum in the system resides in the collective $k = 0$ mode (taken to be aligned with the \tilde{z} axis) and higher order terms in the Holstein-Primakoff transformation can be ignored. The system's dynamics can then be described as that of the collective spin on a Bloch sphere with a small density of spin-waves, negligibly reducing the length of this collective magnetization. TDSW is valid up to times $\sim 1/\epsilon^2$ [37]; accordingly, the dynamics illustrated in the main text are faithfully described as they satisfy $\epsilon(t) \lesssim 0.2$. The ‘time-dependent’ part of TDSW references choosing the rotating frame angles $\theta(t)$ and $\phi(t)$ at every momentum in time so that the \tilde{z} axis aligns with the collective spin, which amounts to determining the equations of motion for these angles by enforcing $\langle S_{k=0}^{\tilde{x}} \rangle = 0$ and $\langle S_{k=0}^{\tilde{y}} \rangle = 0$. The position of the collective spin on the Bloch sphere defined in the lab frame is given as $\vec{m} = (m^x, m^y, m^z)$ where

$$m^x(t) = \sin \theta(t) \cos \phi(t), \quad m^y(t) = \sin \theta(t) \sin \phi(t), \quad m^z(t) = \cos \theta(t). \quad (\text{S.47})$$

This choice extends the validity of spin-wave theory to larger window of dynamics by redefining the spin-wave vacuum, represented by the collective spin, at every point in time so that the total spin-wave density on top of the vacuum remains small. In the dilute regime of $\epsilon(t) \ll 1$, spin waves behave as free bosonic modes which scatter self-consistently only with the collective magnetization ($k = 0$ mode).

We apply the Holstein-Primakoff transformation described above to the adjoint master equation Eq.S.34. A sufficiently small spin-wave density allows us to truncate the equations of motion for the system at the Gaussian level; we expect the expectation value of operators that are more than quadratic in spin-wave operators to be negligible in this limit. This approximation then allows for a closed set of non-linear coupled dynamical equations involving only the angles $\theta(t)$ and $\phi(t)$, representing the one-point correlation functions, and the two-point correlation functions defined below:

$$\Delta_k^{qq}(t) = \langle \hat{q}_k(t) \hat{q}_{-k}(t) \rangle, \quad \Delta_k^{pp}(t) = \langle \hat{p}_k(t) \hat{p}_{-k}(t) \rangle, \quad \Delta_k^{qp}(t) = \frac{1}{2} \langle \hat{q}_k \hat{p}_{-k} + \hat{p}_k \hat{q}_{-k} \rangle. \quad (\text{S.48})$$

The dynamics of these two-point functions act as feedback for the motion of $\theta(t)$ and $\phi(t)$.

Specifically, we substitute the spin operators with bosonic creation and annihilation operators in the Hamiltonian or dissipator and keep contributions that are at most quadratic in bosonic operators. We then substitute quadrature

operators for the creation and annihilation operators before computing equations of motion for $\hat{q}_{k=0}$, $\hat{p}_{k=0}$, $\hat{q}_k \hat{q}_{-k}$, $\hat{p}_k \hat{p}_{-k}$, and $\frac{1}{2}(\hat{q}_k \hat{p}_{-k} + \hat{p}_k \hat{q}_{-k})$. The first two quantities and enforcement of $\langle S_{k=0}^{\tilde{x}} \rangle = \langle S_{k=0}^{\tilde{y}} \rangle = 0$ yields equations of motion for the angles $\theta(t)$ and $\phi(t)$ respectively, while the latter three quantities yield equations of motion for the two-point functions given in Eq.S.48. It is important to note three technical points. First, we must do the Gaussian approximation in terms of bosonic creation and annihilation operators rather than quadratures as $\hat{b}_k^\dagger \hat{b}_k$ is the quantity that is related to the small parameter ε that we are expanding around; doing the approximation in terms of quadrature operators may yield spurious terms in the final equations due to zero-point quantum fluctuations. Second, we must apply the Holstein-Primakoff transformation and Gaussian approximation at the level of the generators Eqs.S.37-S.39 before calculating the equation of motion for an operator \hat{A} ; performing the Gaussian approximation after computing the equation of motion may also introduce spurious terms in the final equations. Third, the Leibniz rule for derivatives does not apply to operators evolving under a Lindblad master equation so the equations for the two-point functions must be directly computed; we cannot construct these equations from a product of the equations of motion for the one-point functions as is commonly done when TDSW is applied to purely unitary systems.

C. Equations of motion

The equations of motion for the system are then assembled as follows. First, we start with the contributions of the Larmor Hamiltonian \hat{H}_{RF} which will always be present due to the rotation of the reference frame:

$$\frac{d}{dt} \theta = 0 \quad (\text{S.49})$$

$$\frac{d}{dt} \phi = 0 \quad (\text{S.50})$$

$$\frac{d}{dt} \Delta_k^{qq} = \cos \theta \dot{\phi} (2\Delta_k^{qp}) \quad (\text{S.51})$$

$$\frac{d}{dt} \Delta_k^{pp} = -\cos \theta \dot{\phi} (2\Delta_k^{qp}) \quad (\text{S.52})$$

$$\frac{d}{dt} \Delta_k^{qp} = -\cos \theta \dot{\phi} (\Delta_k^{qq} - \Delta_k^{pp}) \quad (\text{S.53})$$

Each channel j , given by a choice of one of the generators in Eqs.S.37-S.39, then contributes to the above equations as

$$\frac{d}{dt} \theta \rightarrow \frac{d}{dt} \theta + d\theta_j \quad (\text{S.54})$$

$$\frac{d}{dt} \phi \rightarrow \frac{d}{dt} \phi + d\phi_j \quad (\text{S.55})$$

$$\frac{d}{dt} \Delta_k^{qq} \rightarrow \frac{d}{dt} \Delta_k^{qq} + dQ_j \quad (\text{S.56})$$

$$\frac{d}{dt} \Delta_k^{pp} \rightarrow \frac{d}{dt} \Delta_k^{pp} + dP_j \quad (\text{S.57})$$

$$(\text{S.58})$$

$$\frac{d}{dt} \Delta_k^{qp} \rightarrow \frac{d}{dt} \Delta_k^{qp} + dW_j \quad (\text{S.59})$$

Below we give the contributions to the equations of motion from each type of channel. It is useful to define the quantities

$$\xi_{\tilde{\alpha},\tilde{\beta}} = \frac{M_{\tilde{\beta},\tilde{\alpha}}}{M_{\tilde{\alpha},\tilde{\beta}}} = \frac{M_{\tilde{\alpha},\tilde{\beta}}^*}{M_{\tilde{\alpha},\tilde{\beta}}} \quad (\text{S.60})$$

$$\delta^{\eta\xi} = \frac{1}{\Gamma_{k=0} N s} \sum_{k \neq 0} \Gamma_k \Delta_k^{\eta\xi}. \quad (\text{S.61})$$

The contributions from a \hat{H}_F channel are

$$d\theta_{H_F} = \omega_F F_{\tilde{y}} \quad (S.62)$$

$$d\phi_{H_F} = -\omega_F F_{\tilde{x}} \frac{1}{\sin \theta} \quad (S.63)$$

$$dQ_{H_F} = -\omega_F 2F_{\tilde{z}} \Delta_k^{qp} \quad (S.64)$$

$$dP_{H_F} = \omega_F 2F_{\tilde{z}} \Delta_k^{qp} \quad (S.65)$$

$$dW_{H_F} = \omega_F F_{\tilde{z}} (\Delta_k^{qq} - \Delta_k^{pp}) \quad (S.66)$$

The contributions from a \hat{H}_L channel are

$$\begin{aligned} d\theta_{H_L} = & -M_{\tilde{x},\tilde{z}} 4\eta \frac{1}{\Gamma_{k=0} N_s} \sum_{k'} \Gamma_{k'} \frac{1}{2} \langle \hat{q}_{-k'} \hat{p}_{k'} + \xi_{\tilde{x},\tilde{z}} \hat{p}_{-k'} \hat{q}_{k'} \rangle \\ & + M_{\tilde{y},\tilde{z}} 2\eta (1 + \xi_{\tilde{y},\tilde{z}}) \left(1 - \varepsilon - \delta_{\alpha}^{pp} - \frac{1}{N_s} n_{k=0} - \frac{1}{N_s} \Delta_{k=0}^{pp} \right) \end{aligned} \quad (S.67)$$

$$d\phi_{H_L} = M_{\tilde{y},\tilde{z}} \frac{1}{\sin \theta} 4\eta \frac{1}{\Gamma_{k=0} N_s} \sum_{k'} \Gamma_{k'} \frac{1}{2} \langle \hat{p}_{-k'} \hat{q}_{k'} + \xi_{\tilde{y},\tilde{z}} \hat{q}_{-k'} \hat{p}_{k'} \rangle \quad (S.68)$$

$$- M_{\tilde{x},\tilde{z}} \frac{1}{\sin \theta} 2\eta (1 + \xi_{\tilde{x},\tilde{z}}) \left(1 - \varepsilon - \delta_{\alpha}^{qq} - \frac{1}{N_s} n_{k=0} - \frac{1}{N_s} \Delta_{k=0}^{qq} \right) \quad (S.69)$$

$$dQ_{H_L} = M_{\tilde{y},\tilde{y}} \eta \cdot 8 \frac{\Gamma_k}{\Gamma_{k=0}} \Delta_k^{qp} - M_{\tilde{z},\tilde{z}} \eta \cdot 8 \Delta_k^{qp} + M_{\tilde{x},\tilde{y}} 4\eta (1 + \xi_{\tilde{x},\tilde{y}}) \frac{\Gamma_k}{\Gamma_{k=0}} \Delta_k^{qq} \quad (S.70)$$

$$dP_{H_L} = -M_{\tilde{x},\tilde{x}} \eta \cdot 8 \frac{\Gamma_k}{\Gamma_{k=0}} \Delta_k^{qp} + M_{\tilde{z},\tilde{z}} \eta \cdot 8 \Delta_k^{qp} - M_{\tilde{x},\tilde{y}} 4\eta (1 + \xi_{\tilde{x},\tilde{y}}) \frac{\Gamma_k}{\Gamma_{k=0}} \Delta_k^{pp} \quad (S.71)$$

$$dW_{H_L} = -M_{\tilde{x},\tilde{x}} \eta \cdot 4 \frac{\Gamma_k}{\Gamma_{k=0}} \Delta_k^{qq} + M_{\tilde{y},\tilde{y}} \eta \cdot 4 \frac{\Gamma_k}{\Gamma_{k=0}} \Delta_k^{pp} \quad (S.72)$$

$$+ M_{\tilde{z},\tilde{z}} \eta \cdot 4 (\Delta_k^{qq} - \Delta_k^{pp}) \quad (S.73)$$

The contributions from a \mathcal{D}_L channel are

$$d\theta_{\mathcal{D}_L} = -i M_{\tilde{x},\tilde{z}} \frac{1}{2} \kappa \frac{1}{\Gamma_{k=0} N_s} \sum_{k'} \Gamma_{k'} \langle \hat{q}_{-k'} \hat{p}_{k'} - \xi_{\tilde{x},\tilde{z}} \hat{p}_{k'} \hat{q}_{-k'} \rangle \quad (S.74)$$

$$- i M_{\tilde{y},\tilde{z}} \frac{1}{2} \kappa (1 - \xi_{\tilde{y},\tilde{z}}) \left(1 - \varepsilon + \delta_{\alpha}^{pp} - \frac{1}{N_s} n_{k=0} + \frac{1}{N_s} \Delta_{k=0}^{pp} \right) \quad (S.75)$$

$$d\phi_{\mathcal{D}_L} = i M_{\tilde{y},\tilde{z}} \frac{1}{\sin \theta} \frac{1}{2} \kappa \frac{1}{\Gamma_{k=0} N_s} \sum_{k'} \Gamma_{k'} \langle \hat{p}_{-k'} \hat{q}_{k'} - \xi_{\tilde{y},\tilde{z}} \hat{q}_{k'} \hat{p}_{-k'} \rangle \quad (S.76)$$

$$+ i M_{\tilde{x},\tilde{z}} \frac{1}{\sin \theta} \frac{1}{2} \kappa (1 - \xi_{\tilde{x},\tilde{z}}) \left(1 - \varepsilon + \delta_{\alpha}^{qq} - \frac{1}{N_s} n_{k=0} + \frac{1}{N_s} \Delta_{k=0}^{qq} \right) \quad (S.77)$$

$$dQ_{\mathcal{D}_L} = M_{\tilde{y},\tilde{y}} \kappa \frac{\Gamma_k}{\Gamma_{k=0}} + i M_{\tilde{x},\tilde{y}} \kappa (1 - \xi_{\tilde{x},\tilde{y}}) \frac{\Gamma_k}{\Gamma_{k=0}} \Delta_k^{qq} \quad (S.78)$$

$$dP_{\mathcal{D}_L} = M_{\tilde{x},\tilde{x}} \kappa \frac{\Gamma_k}{\Gamma_{k=0}} + i M_{\tilde{x},\tilde{y}} \kappa (1 - \xi_{\tilde{x},\tilde{y}}) \frac{\Gamma_k}{\Gamma_{k=0}} \Delta_k^{pp} \quad (S.79)$$

$$dW_{\mathcal{D}_L} = i M_{\tilde{x},\tilde{y}} \kappa \frac{\Gamma_k}{\Gamma_{k=0}} \frac{1}{2} \langle \hat{q}_k \hat{p}_{-k} - \xi_{\tilde{x},\tilde{y}} \hat{p}_k \hat{q}_{-k} + \hat{q}_{-k} \hat{p}_k - \xi_{\tilde{x},\tilde{y}} \hat{p}_{-k} \hat{q}_k \rangle \quad (S.80)$$

Note that the spin-wave density is expressed in terms of two-point correlation functions as $\varepsilon(t) = \frac{1}{Ns} \sum_{k \neq 0} n_k$ where $n_k = \frac{1}{2} (\Delta_k^{qq} + \Delta_k^{pp} - 1)$. After assembling the contributions of each desired channel to the equations of motion for the collective spin angles and two-point functions, we then plug in the final expression for $\frac{d}{dt} \phi$ into the Larmor term in the equations of motion for the two-point functions. We then keep terms that are second order in $k \neq 0$ spin-wave operators. As each Larmor term is proportional to $\frac{d}{dt} \phi$ multiplied by a two-point function, we only keep terms in $\frac{d}{dt} \phi$ that are zeroth order in spin-wave operators when substituting the expression. In the above expressions, we have kept terms that are proportional to $\frac{1}{Ns}$ which are necessary to quantify finite size effects. In the thermodynamic limit, these terms vanish. The treatment thus results in a set of differential equations for the collective angles $\theta(t)$ and $\phi(t)$ which are coupled to the $2N$ equations of motion for the two-point correlation functions which represent the dynamics of spin-wave excitations. The coupling between these equations represents the self-consistent part of the method where the quantum fluctuations of spin-waves affects the motion of the spin-wave vacuum and vice-versa.

D. Observables

Common quantities of interest are equal time spin-spin correlation functions and spin squeezing parameters. We give expressions for these quantities in terms of the collective spin angles and the spin-wave two-point functions computed above. Let us define the equal time correlation function

$$C^{\alpha\alpha}(r, t) \equiv \langle \hat{S}_n^\alpha(t) \hat{S}_{n+r}^\alpha(t) \rangle - \langle \hat{S}_n^\alpha(t) \rangle \langle \hat{S}_{n+r}^\alpha(t) \rangle \quad (\text{S.81})$$

where α describes a direction in the lab frame. In terms of TDSW variables, the correlation function is computed as

$$C^{\alpha\alpha}(r, t) = (G_{\tilde{x}, \alpha})^2 \frac{s}{N} \sum_{k \neq 0} e^{-ikr} \Delta_k^{qq} + (G_{\tilde{y}, \alpha})^2 \frac{s}{N} \sum_{k \neq 0} e^{-ikr} \Delta_k^{pp} + 2G_{\tilde{x}, \alpha} G_{\tilde{y}, \alpha} \frac{s}{N} \sum_{k \neq 0} e^{-ikr} \Delta_k^{qp}. \quad (\text{S.82})$$

Let us define the squeezing parameter

$$\xi_k^2 \equiv \frac{\min_{e_\perp} \langle \Delta \left(e_\perp \cdot \hat{\vec{S}}_k \right)^2 \rangle}{\frac{1}{2} \frac{N}{2}} \quad (\text{S.83})$$

where we are minimizing the variance $\langle \Delta \left(e_\perp \cdot \hat{\vec{S}}_k \right)^2 \rangle = \langle (e_\perp \cdot \hat{\vec{S}}_k)^2 \rangle - \langle e_\perp \cdot \hat{\vec{S}}_k \rangle^2$ over directions e_\perp perpendicular to the mean spin direction $e_{\bar{m}} \equiv \frac{\langle \hat{\vec{S}}_k \rangle}{|\langle \hat{\vec{S}}_k \rangle|}$ of the spin mode at wavevector k . For $k = 0$, $\hat{\vec{S}}_{k=0}$ is the total spin operator and $\xi_{k=0}$ is the usual Kitagawa squeezing parameter [43]. In the TDSW treatment, this total spin points in the direction of the rotating \tilde{z} -axis and the squeezed quadratures are computed on the tangent plane at the intersection of the collective spin and the Bloch sphere. As discussed, in the main text, the $\xi_{k \neq 0}$ is related to spatial entanglement and may be pertinent to spatially resolved metrology. We can also define the squeezing parameter

$$\xi_{W,k}^2 \equiv \left(\frac{N/2}{|\langle \hat{\vec{S}}_k \rangle|} \right)^2 \xi_k^2 \quad (\text{S.84})$$

which for $k = 0$ is Wineland's squeezing parameter which is directly related to metrological applications [43]. In terms of TDSW variables, the Kitagawa parameter is expressed as

$$\xi_k^2 = 1 + 2n_k - 2\sqrt{n_k(1+n_k) + \Delta_k^{SR}} \quad (\text{S.85})$$

where $\Delta_k^{SR} \equiv \frac{1}{4} - \Delta_k^{qq} \Delta_k^{pp} + (\Delta_k^{qp})^2$. For a purely unitary dynamics where we assume the system is in a pure Gaussian state, we have $\Delta_k^{SR} = 0$. For a mixed state undergoing Lindblad dynamics, this is generally not true even under the Gaussian approximation. The Wineland parameter is expressed as

$$\xi_{W,k}^2 = \frac{1}{(1-\varepsilon)^2} \xi_k^2. \quad (\text{S.86})$$

We can also define the quantity

$$\xi^2(r) \equiv \frac{1}{s} \min_{e_\perp} \langle \Delta \left(e_\perp \cdot (\hat{\vec{S}}_{n+r} - \hat{\vec{S}}_n) \right)^2 \rangle \quad (\text{S.87})$$

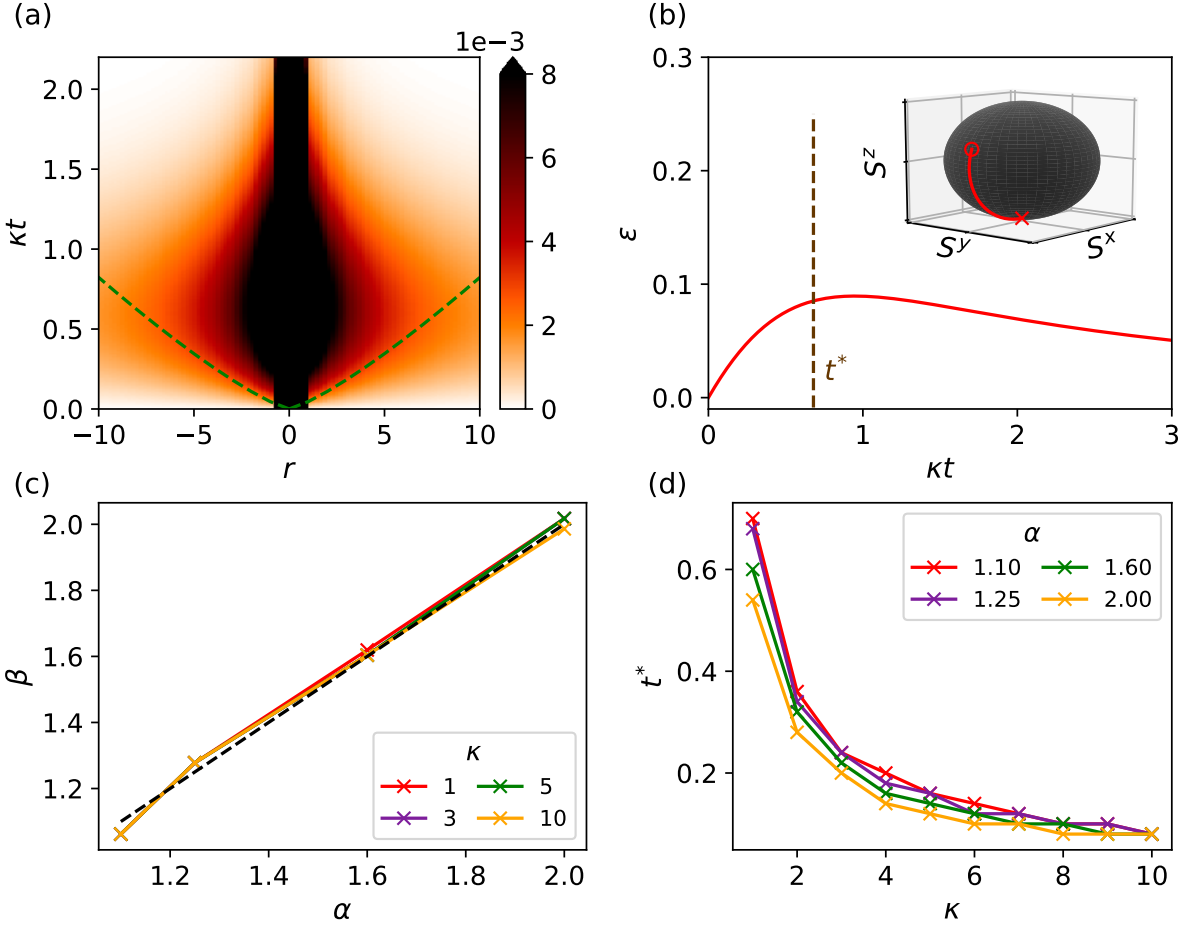


Figure S4. **Dynamics of $\hat{L}_n = \hat{S}_n^-$ dissipation with long-range spatial profile $f(|r|) = (|r| + 1)^{-\alpha}$.** (a) Spreading and contraction of spin correlations for $\alpha = 1.25$ and $\kappa = 1.0$; the green dotted line tracks the correlation front which spreads as $t \approx r^\beta$ at short times. (b) Dynamics of the spin wave density and evolution of the collective magnetization on the Bloch sphere (inset) for the same choice of parameters as (a). The density of spin waves has a peak at time t^* where the front of correlations reverses (cf. (a)). (c) Scaling parameter β as a function of α . The black dotted line represents $\beta = \alpha$; we see that $\beta \simeq \alpha$ independent of the dissipation strength κ . (d) Dependence of t^* on α and κ . For all panels we evaluate dynamics in the thermodynamic limit with the initial state of the system representing a spin coherent state pointing in the direction $\theta(t=0) = 0.4\pi$, $\phi(t=0) = 0$.

which tells us the uncertainty when measuring the correlation between spins that are a fixed distance r apart. In terms of TDSW variables, this quantity is expressed as

$$\xi^2(r) = \frac{1}{N} \sum_k (1 - \cos(kr)) \xi_k^2. \quad (\text{S.88})$$

Note that the $k = 0$ term does not contribute to the sum above and so $\xi^2(r)$ is related purely to spatial correlations of the system. If we have a system such that $\xi_{k \neq 0}^2 = \xi_K^2$ does not depend on k , then $\lim_{r \rightarrow \infty} \xi^2(r) = \xi_K^2$ and a measurement of $\xi^2(r)$ can be used to infer ξ_K^2 . Such a measurement can be performed by applying a global rotation on the system to align the e_z -axis with the e_\perp axis, and then projectively measuring in the z -basis using fluorescence imaging.

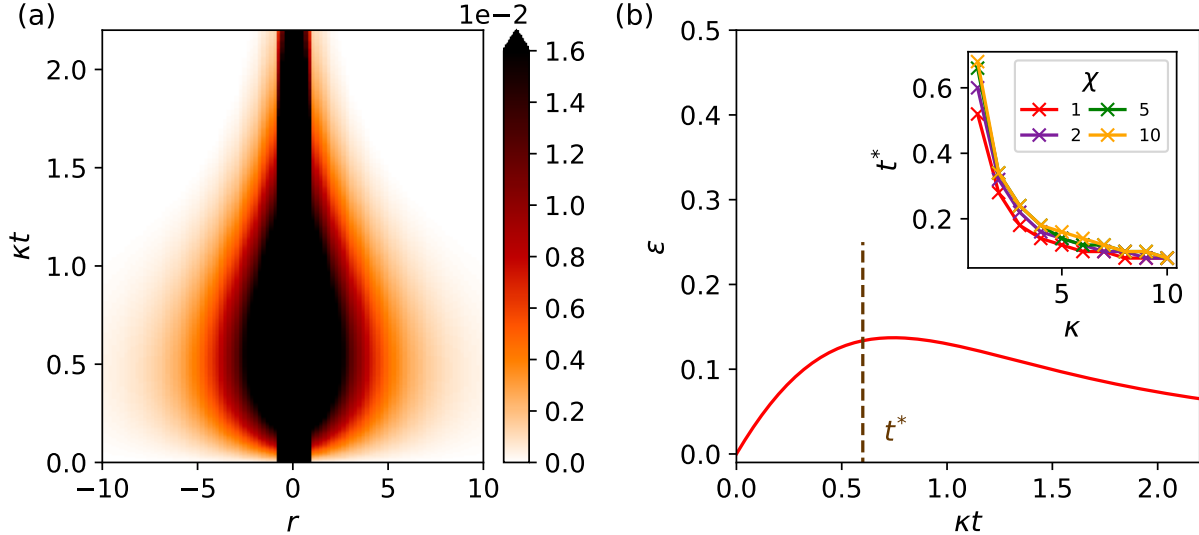


Figure S5. **Dynamics of $\hat{L}_n = \hat{S}_n^-$ dissipation with short-range spatial profile $f(|r|) = \exp(-|r|/\chi)$.** (a) Spreading and contraction of spin correlations for $\chi = 2.0$ and $\kappa = 1.0$. (b) Dynamics of spin-wave density and correlation function transition time (inset). For all panels we evaluate dynamics in the thermodynamic limit with the initial state of the system representing a spin coherent state pointing in the direction $\theta(t=0) = 0.4\pi$, $\phi(t=0) = 0$.

S3. DYNAMICS OF CORRELATION FUNCTIONS FOR SHORT- AND LONG-RANGE LOSSES

In this section, we further analyze the dynamics of the $\hat{L}_n = \hat{S}_n^-$ dissipation channel described in Eq. (1) of the main text. Specifically, we consider a Lindblad channel

$$\mathcal{D}_L(\hat{A}) = \frac{\kappa}{s\Gamma_{k=0}} \sum_{n,m} f(|n-m|) \left(\hat{S}_n^+ \hat{A} \hat{S}_m^- - \frac{1}{2} \{ \hat{S}_m^+ \hat{S}_n^-, \hat{A} \} \right) \quad (\text{S.89})$$

with long-range and short-range spatial profiles given respectively by

$$f(|n-m|) = (|n-m|+1)^{-\alpha} \text{ and } f(|n-m|) = \exp(-|n-m|/\chi). \quad (\text{S.90})$$

Recall that $\Gamma_k \equiv \sum_{r \in \{-\frac{N}{2}, \frac{N}{2}\}} e^{ikr} f(|n-m|)$ is the Fourier transform of the spatial profile and that the factor of $\Gamma_{k=0}$ is the Kac renormalization of the channel. We note that Eq. (1) of the main text is given without this normalization for the sake of clarity, but the figures in the main text, including the definition of κ for the parameter values given, correspond to the channel defined in Eq. (S.89).

Using the formalism of time-dependent spin-wave theory as described in Sec. S2, we can derive a differential equation for the occupation n_k of the spin-wave excitation at wavevector $k \neq 0$.

$$\frac{d}{dt} n_k = 2\kappa \frac{\Gamma_k}{\Gamma_{k=0}} \left(n_k \cos \theta(t) + \cos^4 \left(\frac{\theta(t)}{2} \right) \right). \quad (\text{S.91})$$

The k -dependent prefactor $\Gamma_k/\Gamma_{k=0}$ is positive for both spatial profiles of interest and we take κ to be positive. Remarkably, Eq. S.91 is a linear differential equation that is not coupled to other TDSW variables; this is not true for a general dynamical channel. The homogeneous term in Eq. (S.91) describes the rate of production of spin-waves and depends on $\cos \theta(t)$; accordingly, it generates or drains spin waves depending on whether the collective magnetization is in the northern ($0 < \theta(t) < \pi/2$) or southern ($\pi/2 < \theta(t) < \pi$) hemisphere of the Bloch sphere. In other words, the transition in the rate of production of spin waves can be understood as a consequence of the spin waves' dynamics being dependent on the instantaneous mean field represented by the collective spin. While the effect of dissipation is creating spin waves on top of a mean field in the northern hemisphere, the same dissipative mechanism results in a reduction of spin-waves with respect to a mean-field in the southern hemisphere.

Note that this behavior is a result of the choice of dissipation channel, $\hat{L}_n = \hat{S}_n^-$, and does not depend on the choice of spatial profile which only modifies the prefactor $\Gamma_k/\Gamma_{k=0}$ in Eq (S.91). Panels (c) and (f) of Fig. S2 show the form of this prefactor for long-range and short-range spatial profiles respectively. The long-range profile is a

power-law decay characterized by power α and results in a prefactor that decays as a power-law with power related to α . The short-range profile is an exponential decay characterized by a decay length χ and results in a prefactor that is Lorentzian with width proportional to $1/\chi$. The change in spatial profile determines modifications in some non-universal parameters such as the transition time, t^* upon which the system switches from pumping excitations to draining excitations. The spatial profile is, however, important when engineering the dynamics of the system for certain applications. For example, the squeezing at a given wavevector k , given by Eq. S.85, increases as the spin-wave occupation increases. If we want to preferentially squeeze a given mode k^* , then we would like the occupation of that mode to grow much faster than other modes. This can be done by choosing the spatial profile such that Γ_k is peaked around $k = k^*$. For example, if we choose $f(|n - m|) = \cos(k^*|n - m|)\exp(-|n - m|/\chi)$, its Fourier transform Γ_k is a Lorentzian peaked at k^* with width $1/\chi$. Such a choice would make squeezing of the k^* mode grow faster than the squeezing of other modes, thereby allowing preferentially entanglement at a desired spatial resolution length.

The mechanism governing the dynamics of spin-wave occupation is also responsible for the dynamics of equal time spin-spin correlation functions. As an example, we examine the correlation function

$$C^{zz}(r, t) = \langle \hat{S}_n^z(t) \hat{S}_{n+r}^z(t) \rangle - \langle \hat{S}_n^z(t) \rangle \langle \hat{S}_{n+r}^z(t) \rangle \quad (\text{S.92})$$

which is directly sensitive to the action of spin losses $\hat{L}_n = \hat{S}_n^-$. This function can be expressed in terms of TDSW variables as

$$C^{zz}(r, t) = (\sin \theta(t))^2 \sum_{k \neq 0, k > 0} \cos(kr) \Delta_k^{qq}. \quad (\text{S.93})$$

We see that there is an overall envelope to the correlation dynamics set by $[\sin \theta(t)]^2$, which grows as the collective spin moves from the north pole of the Bloch sphere to the equator, and shrinks as it moves from the equator to the south pole. Therefore, in the absence of other dynamical channels, we expect the correlations to grow for a period of time and then shrink, with the time t^* upon which the system transitions between these two regimes being dependent on the motion of the collective spin. As the dynamics of spin-wave occupation also increases and decreases depending on the collective spin motion, we expect that the correlation transition time t^* sets the scale upon which the spin-wave density ε reaches its maximum value before shrinking. Similar to the dynamics of spin-wave occupation, we note that the choice of spatial profile does not qualitatively modify the correlation dynamics. The spatial profile only enters Eq. S.93 through the dynamics of Δ_k^{qq} .

We now numerically calculate the dynamics of the correlation function, Eq. S.93, using TDSW and analyze both long-range and short-range cases. We start with all the spins in a coherent state pointing slightly above the equator of the Bloch sphere ($\theta(t=0) = 0.4\pi$, $\phi(t=0) = 0$). The qualitative nature of the dynamics for this dissipative channel does not depend on the angle of the initial coherent state; starting too close to the North pole, however, causes the spin-wave density to exceed the threshold treatable by TDSW. Our choice of $\theta(t=0) = 0.4\pi$ allows the dynamics to be validly treated with TDSW.

The correlation dynamics for the long-range spatial profile is shown in Fig. S4(a). In the first stage of dynamics, correlations exhibit a front scaling as $t \approx r^\beta$. The exponent β is plotted in Fig. S4(c), showing that the dissipation strength κ does not play a role in the ‘opening’ of the correlation function. The exponent β characterizing the scaling follows $\beta \simeq \alpha$; this result can be understood by making the following scaling ansatz for $C^{zz}(r, t)$ in the initial opening stage of correlation spreading dynamics:

$$C^{zz}(rt_1^{1/\beta}, t_1) = C^{zz}(rt_2^{1/\beta}, t_2). \quad (\text{S.94})$$

Algebraic manipulation yields the equivalent expressions

$$\begin{aligned} C^{zz}(\zeta r, t) &= \zeta^\nu C^{zz}(r, t), \\ C^{zz}(r, \zeta t) &= \zeta^{-\nu\eta} C^{zz}(r, t). \end{aligned} \quad (\text{S.95})$$

Here ζ is a positive rescaling factor while ν and η are the two rescaling exponents for space and time. The above ansatz represents a correlation function front scaling with exponent $\beta = 1/\eta$. As we discuss later, we find that for large distances ($r \gg 1$), the correlation function satisfies $C^{zz}(r, t) \propto 1/r^\alpha$. This behavior yields $\nu = -\alpha$ using the first equation in (S.95). Additionally, at short times, correlations grow linearly to leading order ($C^{zz}(r, t \rightarrow 0) \propto t + \mathcal{O}(t^2)$) as we start with an uncorrelated spin coherent state for which $C^{zz}(r, t=0)$ is vanishing. The second equation in (S.95) therefore implies $\nu\eta = -1$, and combining these conditions yields $\eta = 1/\alpha$. We therefore see that the correlation front must scale as $t \simeq r^\beta$ with $\beta = \alpha$ as numerically observed. At large α , correlations disappear ($\beta \rightarrow \infty$) consistently with the Lindbladian becoming diagonal and representing independent local emission events. This behavior differs from the large α light cone of long-range Hamiltonians which becomes increasingly linear ($\beta \approx 1$) [44]. As stated in

Sec. S2, this difference arises from the proper way to define long-range dissipation ($f(|n - m|) = (|n - m| + 1)^{-\alpha}$) versus coherent dynamics ($f(|n - m|) = |n - m|^{-\alpha}$). In the former case, we tend towards independent dissipators for large α , while in the latter case one retrieves nearest-neighbor interactions.

At late times, long-range dissipation has a contractive effect on correlation dynamics. Correlations reach their maximum spread at a time t^* where the spin wave density exhibits a peak. Spin waves are pumped by the second term in the right hand side of Eq. (S.91) which acts as parametric drive, and they are damped by the first term of (S.91) as soon as the collective magnetization enters the southern hemisphere. For sufficiently strong dissipation, the collective magnetization will always eventually enter the southern hemisphere as the south pole is the dark state for strong spin losses. The competition of this self-pumping mechanism and the incoherent depolarization of spins is what leads to the opening and closing of the correlation function. The transition time t^* corresponds to the timescale upon which the spin wave damping term starts to dominate dynamics (see Fig. S4(d)). Correlations vanish in the absence of spin wave excitations and therefore the correlation function $C^{zz}(r, t)$ shrinks to zero as spin waves are progressively dissipated into the environment for $t > t^*$ (see Fig. S4(b)). At sufficiently late times ($t \gg t^*$), there is negligible spin wave density and the system is almost in a coherent state of spins pointing in a direction near the south pole. Closer inspection into the correlations near the steady state shows that $C^{zz}(r) \propto 1/r^\alpha$ for large inter-spin distances. In fact, this $1/r^\alpha$ decay of correlations appears to hold at all times. We also examine the correlation dynamics for a short-range spatial profile. Figure S5(a) shows that the correlations follow the same qualitative behavior as the the long-range case (they grow for a period before contracting). The time t^* characterizing this transition is shown in Fig. S5(b) and it corresponds to the time upon which spin-wave excitations reach their maximal value and start decreasing. In both long- and short-range cases, the time scale t^* increases for spatial profiles that decay more slowly in space. However, the dependence on spatial profile is weak and the transition time primarily depends on the decay rate κ which sets the overall time-scale of the dissipation channel. The main difference between long- and short-range dissipative dynamics is that the correlations decay more rapidly in space for the short-range case, as seen by comparing Fig. S4(a) to Fig. S5(a).